

Swarthmore College

Works

Senior Theses, Projects, and Awards


Student Scholarship

Spring 2017

EPR Studies of Curvature-Dependent Conformational Equilibrium in Full-Length Influenza A M2 Protein

D. Stuart Arbuckle Jr, '17

Follow this and additional works at: <https://works.swarthmore.edu/theses>

 Part of the [Chemistry Commons](#)

Recommended Citation

Arbuckle, D. Stuart Jr, '17, "EPR Studies of Curvature-Dependent Conformational Equilibrium in Full-Length Influenza A M2 Protein" (2017). *Senior Theses, Projects, and Awards*. 224.
<https://works.swarthmore.edu/theses/224>

Please note: the theses in this collection are undergraduate senior theses completed by senior undergraduate students who have received a bachelor's degree.

This work is brought to you for free by Swarthmore College Libraries' Works. It has been accepted for inclusion in Senior Theses, Projects, and Awards by an authorized administrator of Works. For more information, please contact myworks@swarthmore.edu.

EPR Studies of Curvature-Dependent Conformational Equilibrium in Full-Length Influenza A M2 Protein

Presented as a Senior Honors Thesis in Chemistry

D. Stuart Arbuckle, Jr.

Swarthmore College Department of Chemistry and Biochemistry

April 12, 2017

Advisor: Kathleen P. Howard

Abstract:

Matrix 2 (M2) is a homotetrameric integral membrane protein of the influenza A virus demonstrated to be required for generation of membrane curvature resulting in viral budding. The C-terminal amphipathic helix of M2 has been shown to generate negative Gaussian membrane curvature, required at the neck of a budding virion, dependent on membrane composition. In this thesis, electron paramagnetic resonance (EPR) spectroscopy is used to investigate the conformational dynamics of M2's amphipathic helix in liposomes consisting of DOPE and DOPC, lipids of varying intrinsic curvature propensity, as well as cholesterol enrichment. The amphipathic helix is demonstrated to populate two conformations, one of which is stabilized by lipids of high intrinsic curvature propensity or cholesterol. This conformation affects the structure of the amphipathic helix and the transmembrane domain, and is hypothesized to be budding-relevant. Additionally, mutations that alter the budding function of M2 by reducing the hydrophobicity of the amphipathic helix are investigated. Alterations to the helix abolish conformational exchange in response to membrane intrinsic curvature, but not cholesterol, consistent with a role for the amphipathic helix in sensing and responding to membrane curvature properties and binding cholesterol. Changes to the preferred structure as a result of amphipathic helix mutations may explain the recent finding that M2's transmembrane domain is capable of limited curvature generation. The mutated amphipathic helix's conformational dynamics are consistent with a canonical curvature generating/sensing quasi-ALPS motif. The membrane-protein interaction is discussed in the context of the flexible surface model and the spontaneous curvature frustration mechanism, which point to a hydrophobic insertion role for the amphipathic helix that explains lipid-dependent curvature generation.

Attribution and Contributions Statement:

Science is above all a collaborative enterprise and the work presented here is the product of a fruitful collaboration with a number of people.

Chapter 4: Bryan Green '16 conducted preliminary work using the DOPE/DOPC/DOPS lipid system. Megan Thompson '14 conducted much of the overexpression and growths for I51C, F55C, and L59C. Alice Herneisen '17 performed the site directed mutagenesis and purification for the L43R1 and H57R1 sites and assisted with reconstitution. DSA designed experiment, performed purification, reconstitution, and analysis of I51C, F55C and L59C, and performed simulations for all spectra.

Chapter 5: Alice Herneisen '17 conducted purification and assisted in reconstitution of L43R1 and H57R1, and provided power saturation data. DSA designed experiment, processed data, and performed simulations for all spectra.

Chapter 6: The motivation for the penta-Ala mutant study was from the initial work of Alice Herneisen '17, who designed the experiment, overexpressed and purified the protein for the relevant sites in both constructs, and collaborated on reconstitution and data collection and analysis. DSA collaborated on reconstitution, and performed data analysis and simulations.

Ongoing work: Dr. Jimmy Feix (Wisconsin Medical College) conducted preliminary saturation recovery EPR experiments on samples made by Alice Herneisen '17. Dr. Catherine Crouch (Swarthmore College) performed initial dynamic light scattering characterization of proteoliposomes with the assistance of Tyler Alexander '17 on samples made by DSA. Small angle X-ray scattering and electron microscopy work currently being planned will be performed by Dr. Nathan Schmidt (UCSF) and Dr. Catherine Crouch (Swarthmore College), respectively on samples made by DSA.

Table of Contents and Figures

Abstract	2
Attribution and Contribution Statement	2
1. The Influenza A M2 Protein	5
1.1. Motivation: Influenza A M2 protein is a drug target	5
1.2. Structural and functional characterization of M2	5
1.2.1. Figure. Structure and sequence of M2FL	5
1.3. Characterization of M2 amphipathic helix's role in budding	6
2. EPR Theory	8
2.1. SDSL-EPR is a valuable tool for studying membrane proteins	8
2.1.1. Figure. Origin of EPR signal	8
2.1.2. Figure. Attachment of R1 label	9
2.2. SDSL-EPR reveals information about a spin label's chemical environment	10
2.2.1. Figure. Spin label motion	11
2.2.2. Figure. EPR lineshapes	12
2.3. Using SDSL-EPR to identify protein conformational exchange	13
2.3.1. Figure. EPR timescales	14
2.3.2. Figure. Conformational exchange effect on lineshape	15
2.4. Motional model for nitroxide EPR spectral simulation	17
2.4.1. Figure. Definition of the MOMD model	17
2.5. Using SDSL-EPR to measure labelling site solvent accessibility	18
2.6. Using SDSL-EPR to measure inter-label distances	19
3. Materials and Methods	20
3.1. M2FL purification and spin labelling	20
3.2. Selection of lipid mixes and detergent mediated reconstitution	21
3.2.1. Figure. Lipid structures	22
3.3. EPR CW and power saturation collection	22
3.4. EPR analysis and spectral simulation	23
4. Lipid Intrinsic Curvature Propensity Affects Conformational Exchange in Full-Length M2	25
4.1. Background: Role of lipids in generation of membrane curvature	25
4.2. CW EPR lineshapes are multicomponent	25
4.2.1. Figure. EPR lineshapes in different lipid environments	27
4.2.2. Figure. Inverse central line widths	29
4.2.3. Figure. MOMD simulations of EPR spectra in different lipid environments	31
4.2.4. Figure. MOMD model correlation times	33
4.3. Curvature promoted conformation features a more tightly packed and shallower AH	34
4.3.1. Figure. Oxygen power saturation in different lipid environments	34
4.3.2. Figure. Fully/dilute sample ratio distance-dependent dipolar coupling	35
4.4. Curvature results from interplay between M2 and membrane dynamics	36
5. Cholesterol Modulates Lipid Dependent Conformational Exchange in Full-Length M2	41
5.1. M2TMC cholesterol dependent conformational exchange in POPC:POPG	41
5.2. Cholesterol modulates curvature dependent conformational exchange	41
5.2.1. Figure. EPR lineshapes in lipids enriched with cholesterol	44
5.2.2. Figure. Oxygen power saturation for cholesterol samples	45
5.3. Cholesterol-dependent membrane changes at the influenza budzone affecting M2	45
5.4. Spontaneous curvature frustration model for curvature and cholesterol dependent change	48
5.4.1. Figure. Spontaneous curvature frustration relief	51
6. Mutations in the Amphipathic Helix Affect Curvature and Cholesterol Dependent Change	52
6.1. Introduction: Functional relevancy of the penta-Ala mutant AH construct	52
6.2. Curvature and cholesterol dependent change is controlled by amphipathicity	52
6.2.1. EPR lineshapes for wildtype and penta-Ala M2	53
6.2.2. Oxygen power saturation for wildtype and penta-Ala M2	54
6.2.3. MOMD simulations for wildtype and penta-Ala M2	55

6.3. Physical nature of the interaction between M2's AH and the membrane	56
7. Summary and Future Directions	61
7.1. Summary of results and model	61
7.1.1. Figure. Spontaneous curvature frustration model applied to M2 EPR data	61
7.2. Directions for future experiments	62
Acknowledgements	63
Appendix A: Additional Spectra and Simulations	64
Appendix B: MOMD Simulations Parameters	66
Appendix C: Experimental Data Tables	67
Appendix D: Spontaneous Curvature Frustration Model	69

Chapter 1: The Influenza A M2 Protein

1.1. Motivation: Influenza M2 protein is a drug target

Influenza A virus causes regular seasonal epidemics and occasional global pandemics and is responsible for approximately 50,000 global deaths each year, making it a major worldwide public health concern.¹ While vaccination with live-attenuated or inactivated viruses is the preferred method of combatting seasonal influenza, the speed of the virus' mutation combined with the threat of highly virulent pandemic strains and the difficulty of constant virus surveillance has made antiviral drugs an important tool for combatting influenza.² The adamantane antiviral drugs amantadine and rimantadine target matrix 2 (M2); however, virtually all currently circulating strains of influenza A possess the S31N mutation, which confers resistance to these drugs^{3,4}. As a result, the only functional anti-influenza drugs currently available are the neuraminidase inhibitors oseltamivir and zanamivir. Because of the speed of influenza mutation, redundancy in antiviral drug choice is desirable and M2 is an active drug target for development of a replacement antiviral based on a different function of M2.⁵

1.2. Structural and functional characterization of M2

M2 was first discovered and characterized by Robert Lamb and coworkers; the integral viral-membrane associated tetramer of 97-residue monomers comprises an N-terminal extracellular domain, a transmembrane helix, a membrane-associated amphipathic helix, and a C-terminal cytoplasmic tail^{6,7} (Figure 1.2.1). The transmembrane domain forms a pH-dependent ion channel, which has been the subject of most of the structural and functional characterization of M2.^{7,8}

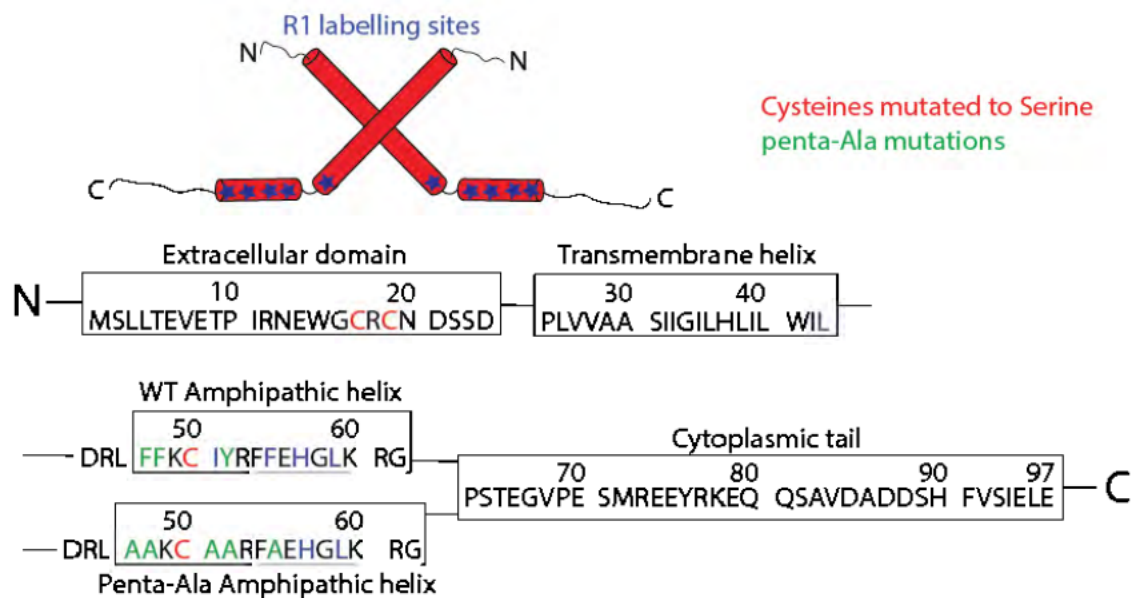


Figure 1.2.1. Structure and sequence of the M2 protein and mutations. Only two monomers of four are shown. Blue represents sites mutated to R1 for EPR studies (section 2.1) while green represents sites mutated to alanine in the penta-Ala construct functional assays. Note that I51 and F55 are both penta-Ala mutated sites and labelling sites in different experiments.

The conformational changes and mechanism of ion channel activity have been elucidated by a variety of methods; the ion channel is activated by protonation of H37, near the binding site of the adamantane drugs. This step is responsible for a structural change in the transmembrane domain between the open and closed channel states.⁴

1.3. Characterization of M2 amphipathic helix's role in viral budding

Mutation studies have determined that the C-terminal cytoplasmic tail of M2 is required for virulence⁹ as well as proper replication.¹⁰ Most notably, mutations in the amphipathic helix part of the cytoplasmic tail abolished proper viral assembly and budding.¹¹ Consistent with the amphipathic helix playing a role in budding and scission, M2 was found to associate with lipid rafts^{12,13} and bind cholesterol.¹⁴ Rossman and coworkers found that cholesterol binding takes place at the amphipathic helix and is crucial for mediating the generation of curvature at the neck of a budding virion. Mutations of five bulky-hydrophobic residues in the

amphipathic helix to alanine (Figure 1.2.1) abolished budding function and presumably destroyed the helix's amphipathic nature. Further, the amphipathic helix was shown to be capable of curvature induction by itself, showing that M2 mediates budding and scission of new virions, bypassing the host endosomal sorting complexes required for transport (ESCRT).^{15,16} Further mutation studies showed that only two of the five hydrophobic sites must be mutated to abolish budding function, showing that the amphipathic helix is crucial for generation of curvature at the viral neck and is highly sensitive to its amphipathicity.¹⁷ Curvature generation by M2 has also been investigated by synchrotron small-angle X-ray scattering (SAXS), showing that the amphipathic helix generates cubic bicontinuous membrane phase, which possesses the same type of curvature observed at the neck of budding virions, in a lipid dependent manner (discussed in greater detail in section 4.2).¹⁸

The goal of this thesis work was to characterize changes to the conformational dynamics of M2's C-terminal amphipathic helix caused by alteration of membrane intrinsic curvature (Chapter 4), cholesterol enrichment (Chapter 5), and functionally relevant mutations to the amphipathic helix (Chapter 6).

Chapter 2. EPR Theory

2.1. SDSL-EPR spectroscopy is a powerful tool for studying membrane proteins

The technique used in this thesis is site directed spin-label electron paramagnetic resonance spectroscopy (SDSL-EPR), which is a powerful tool for probing the conformational dynamics of proteins.¹⁹ EPR shares numerous similarities with nuclear magnetic resonance (NMR) spectroscopy, but is less commonly used and frequently applied to systems not easily characterized by NMR.²⁰ SDSL-EPR has been widely used to study membrane proteins²¹, including M2 by the Howard Group.²²⁻²⁶

Conventional EPR spectroscopy is used to probe the presence and chemical environment of an unpaired electron.²⁷ EPR is largely analogous to NMR except that the latter probes the interaction between the nucleus and an applied magnetic field, while the former probes the interaction between an unpaired electron and an applied magnetic field.²⁷ The spin magnetic moment, μ , and spin angular momentum, S , of an electron are related by the equation, $\mu = g\beta S$, where β is the Bohr magneton and g is the "g-factor" or Zeeman energy.²⁸ In an applied magnetic field, H , solving the Hamiltonian for the interaction between an unpaired electron's spin magnetic moment and the magnetic field yields two wavefunctions with an energy difference between them that is related linearly to H .²⁸ These two wavefunctions can be thought of as representing two states: the electron's spin aligned parallel and antiparallel to the magnetic field.¹⁹ EPR probes this energy difference according to the spectroscopic equation, $\Delta E = h\nu = g|\beta|H$. The EPR spectrometer uses radiation in the form of microwaves of constant frequency and varies H . Such spectra are called continuous wave (CW). An EPR resonance occurs when the energy of the microwaves is equal to the energy difference between the two states of the unpaired electron.¹⁹ The electron

magnetic moment can also interact with a nearby nuclear magnetic moment to produce a hyperfine interaction, resulting in splitting of the EPR resonance into $2I + 1$ peaks, where I is the nuclear spin.²⁸ Since $I = 1$ for ^{14}N , nitroxides commonly used in SDSL-EPR result in three peaks in the EPR signal.²⁷ The requirements for the electron paramagnetic resonance condition are summarized in Figure 2.1.1. EPR signals are typically reported as a first derivative because a smaller field modulation along with the regular field sweep is used in EPR experiments and a first derivative peak achieves a better signal to noise ratio.²⁹

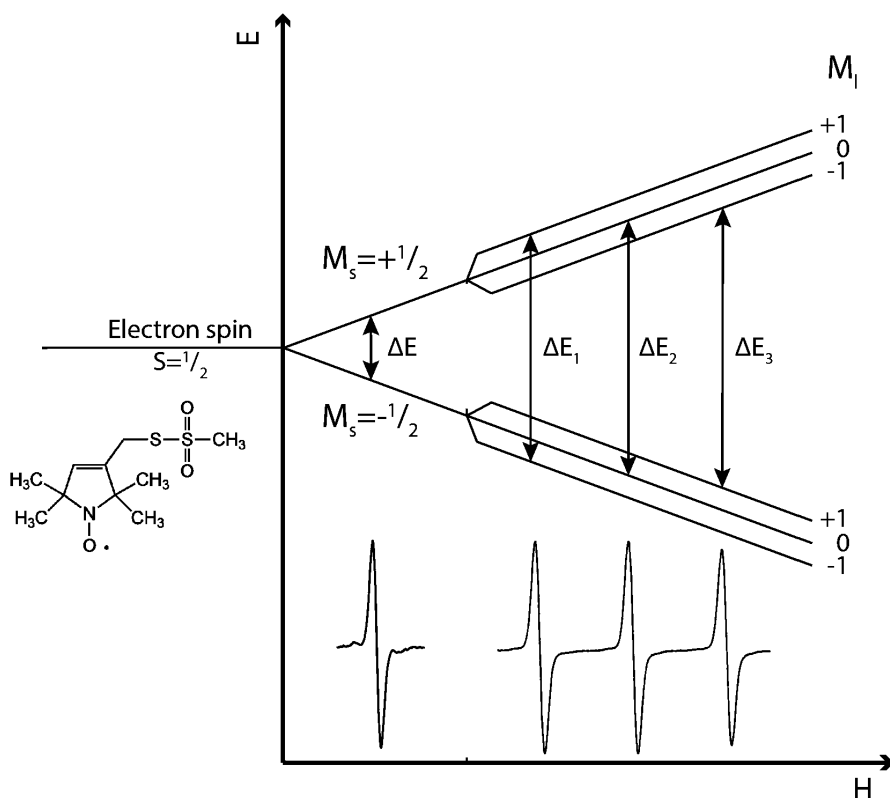


Figure 2.1.1. Origin of the EPR signal for a nitroxide spin label (shown). In the presence of an applied magnetic field, H , the two electron spin states have different energies. The nearby state is further split by the hyperfine interaction with the nucleus. This difference is probed by microwave radiation and the signal is reported as a first derivative.

SDSL-EPR relies on introduction of an unpaired electron to a protein system. The EPR experiments in this thesis utilize the protein-attachable nitroxide label, 2,2,5,5-tetramethyl-1-oxyl-3-methylmethanesulfonate (MTSSL), referred to as R1 when attached to

a protein. A specific residue of the protein is mutated to a cysteine and native cysteines are mutated to serine. MTSSL reacts with cysteine forming a disulfide bond and attaching the R1 nitroxide label to the protein at the selected site, as shown in Figure 2.1.2.

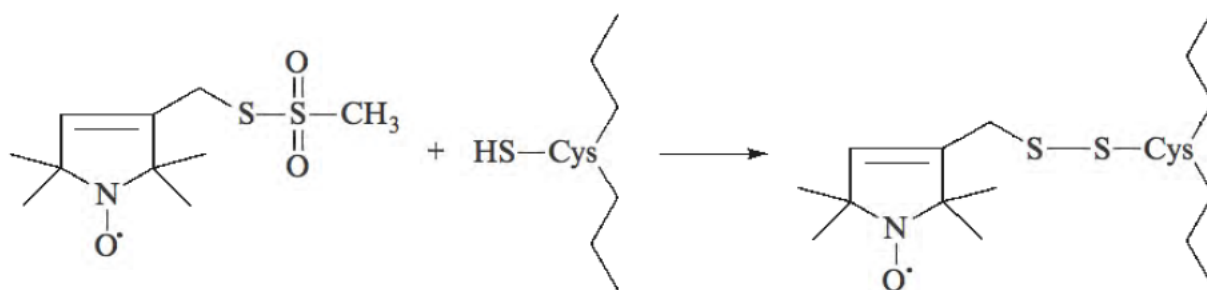


Figure 2.1.2. Disulfide attachment of R1 nitroxide label to the protein. MTSSL reacts with the mutated cysteine to form a covalent attachment of the R1 label to the protein. Figure is reproduced.¹⁹

2.2. SDSL-EPR lineshape reveals information about a spin-label's chemical environment

The most basic information that can be collected from an EPR spectrum is the spectral lineshape.¹⁹ For the X-band (9-10 GHz) spectra included in this thesis, the spectral lineshape reflects the motional freedom of the spin label via the rotational correlation time, τ , which has three components: the overall rotational motion of the protein or protein-complex, the side chain motions, and the backbone fluctuation.²⁰ Lineshape dependence on motional freedom is due to the dependence of the g and A (hyperfine) tensors on the degree of averaging due to motion. For proteins that are sufficiently large (>15 kDa) or for membrane proteins in liposomes, the overall motion of the complex is too slow to affect the EPR lineshape.^{19,20} The focus of analysis of CW EPR lineshapes is on the effect of motion of the spin label side chain.¹⁹ X-ray crystallography, mutational analysis, and NMR studies have established that introduction of the EPR spin-label does not significantly perturb the structure of α helices, and that the most significant contributor to EPR lineshape is side chain motion

rather than fluctuation of the protein backbone.^{19,20,30-32} In an α helix, the R1 label experiences restricted motional freedom due to the formation of a hydrogen bond between the backbone S, sulfur and the side chain C α carbon. This restriction leads to the X₄/X₅ model, in which rotation about only those bonds in the R1 side chain contributes to the motional characteristics of the label.^{20,31,32} Since the unpaired electron of the nitroxide is localized to the N p-orbital, this model leads to motion that may be modeled in a cone, allowing the definition of an order parameter, S, related to the internal motion of the R1 side chain.^{20,30,31} This model is shown graphically in Figure 2.2.1.

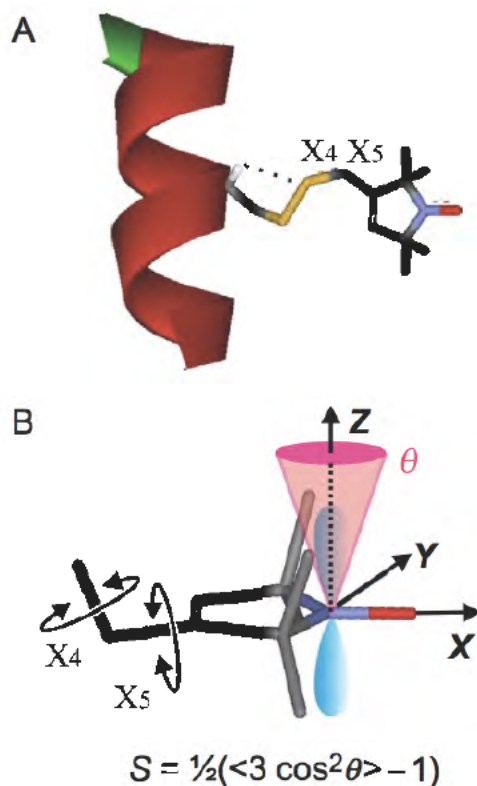


Figure 2.2.1. Motional model for R1 spin label. A.) Rotation about bonds X₄ and X₅ is a result of a hydrogen bond with the protein backbone. B.) These rotations lead to motion of the N p-orbital in a cone, which can be used to define an order parameter, S, related to the motion of the label. Figure is reproduced.²⁰

Although an order parameter is useful for defining the basics of the R1 motional model, in practice the mobility of the label can be inferred by the spectral lineshape itself, which can be simulated (described in section 2.4) to obtain τ . This value for a typical solvent accessible protein labelling site is approximately 2 ns.^{20,28} Figure 2.2.2 demonstrates the effect of R1 mobility on lineshape. Isotropic motion (A) results from fast motion of the spin label in solution and can be used to obtain information about the magnetic tensors of the label's motion.^{20,28,31,33} As the motion of the label is reduced by attachment to unstructured protein (B) or a secondary structure element (C), the lineshape is broadened, corresponding to an increase in τ . Spectra with motion defined by τ are in the slow or intermediate motion regime.^{28,30} The rigid-limit spectrum (D) results from the reduction in motion of the label due to freezing of the sample and can be used to obtain orientation dependent parameters.^{19,20,29}

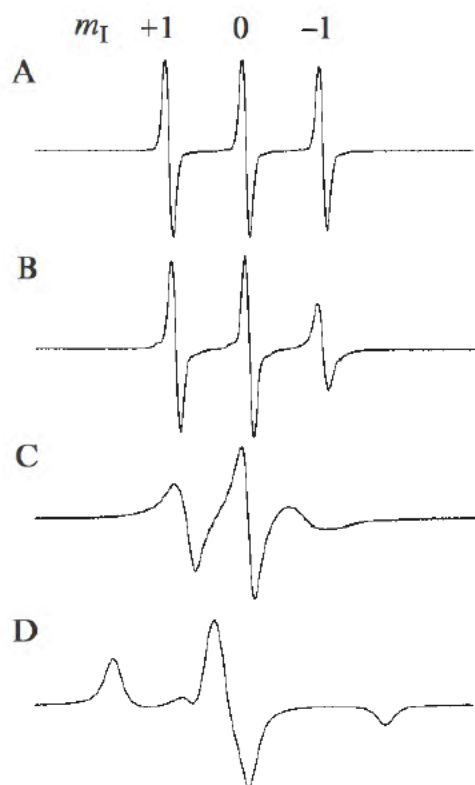


Figure 2.2.2. Effect of R1 motion on CW EPR lineshape. A.) Spin label in solution, B.) attached to unstructured protein, C.) attached to α helix, and D.) in frozen peptide. Figure is reproduced.¹⁹

In most applications of SDSL-EPR, including in this thesis, the internal motion of the spin label side chain is the chief contributor to lineshape.^{19,20} Therefore, the mobility of concern is the rotational correlation time due to these internal motions, τ_i , after this section simply τ . It is possible to interpret spin label CW EPR spectra visually by observing that broader and consequently less intense peaks are characteristic of an immobilized spin label. However, mobility can also be quantified by the central line width at half height, ΔH , which is proportional to τ_i (though it is normally reported as ΔH^{-1} , which is proportional to τ^{-1}).^{19,20,34} For this thesis, spectral simulation (described in section 2.4) is used to obtain τ_i for multiple spectral components due to the presence of conformational exchange.

2.3. Using SDSL-EPR to identify protein conformational exchange

One of the most useful characteristics of SDSL-EPR is the capacity to identify equilibria between protein conformational states. Since protein conformational exchange events occur on a timescale (μs - ms) longer than the characteristic X-band EPR timescale (0.1 - 100 ns), they can usually be well resolved in an EPR spectrum.²⁰ When exchange events are faster (1 - 100 ns) such as fast backbone fluctuations or exchange between statistical substates, the components are spectrally averaged to varying degrees.³⁵ The relationship between the EPR and protein exchange event timescales is demonstrated in Figure 2.3.1.

Protein Exchange Event:

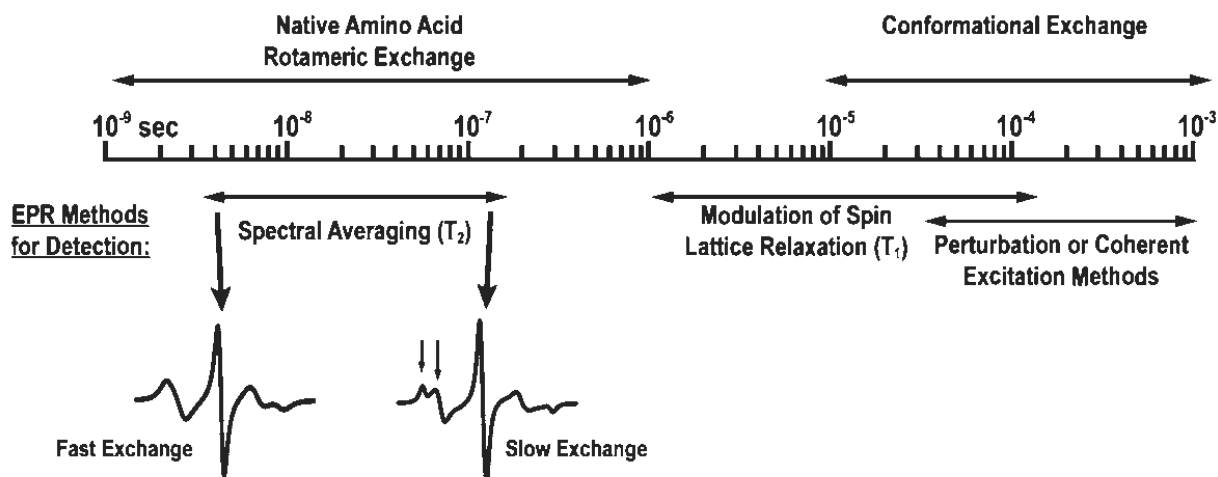


Figure 2.3.1. Relationship between EPR and protein exchange timescales. Slower exchange than the EPR timescale (such as protein conformational exchange) can be resolved while faster exchange events, which include most rotameric exchange, lead to spectral averaging. Figure is adapted.³⁵

When protein conformational exchange events are detected by EPR, the result is a multicomponent (or complex) spectrum. This thesis describes a system in which M2 occupies two different conformations, and spectra represent a weighted average of the two components. Thus, the presence of a characteristic 'double-hump' in the low field CW EPR peak, shown in Figure 2.3.2, typically indicates that the protein undergoes conformational exchange.²⁰ One of the conformations results in a weakly ordered spin label, whereas the other results in immobilization. There are several challenges to the interpretation of multicomponent EPR spectra: Firstly, since SDSL-EPR relies on measurement of the motion of the spin label, conformational exchange is only resolved if the spin-label experiences multiple motional environments, i.e. the conformations translate to different motion of R1 such as weakly ordered and immobilized.^{20,30,31} If the conformations result in the same motion at a particular site, no conformational exchange will be observed at that labelled site. Similarly, if two conformations in a three (or more) conformational system result in the same

mobility at a particular site, they will be resolved to a single component that represents more than one conformation.^{20,36} The second caveat concerns the rotamers of the spin label. Since R1 has access to multiple rotameric states, multicomponent spectra can also result from rotameric exchange, rather than conformational exchange.^{20,35,37} Although rare, this has been demonstrated in a few proteins, thereby showing that rotameric states can have lifetimes of 100 ns or more, long enough that exchange time sensitive experiments (described below) are needed distinguish rotameric from conformational equilibrium.³⁷⁻³⁹

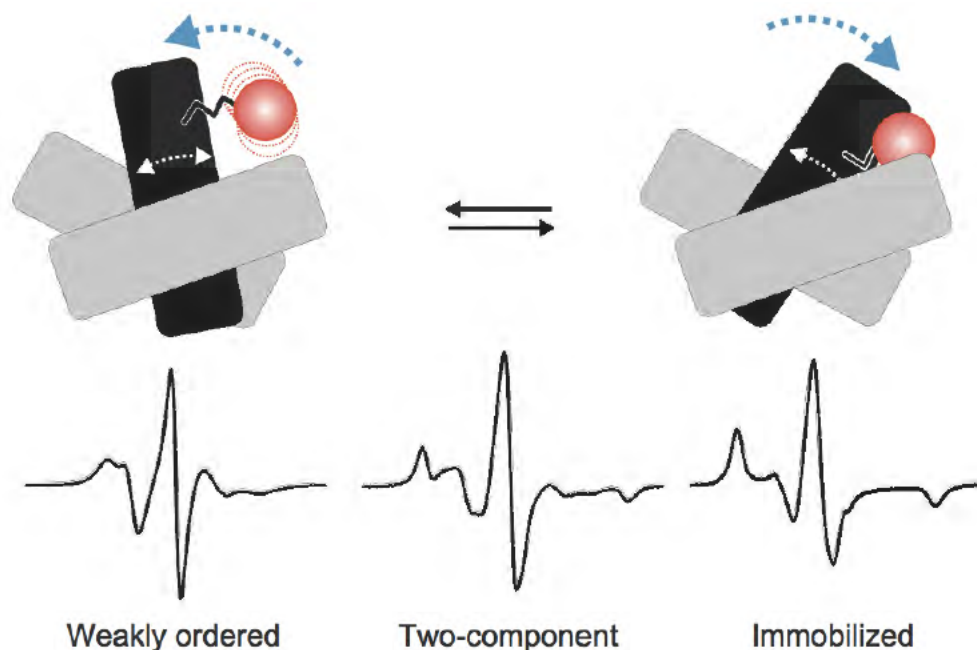


Figure 2.3.2. Multicomponent CW EPR spectrum due to slow conformational exchange. Because this exchange is slower than the EPR timescale, the two motional environments of the spin label (corresponding to two conformations) result in a weighted average two-component spectrum. Figure is reproduced.²⁰

There are multiple experimental techniques for distinguishing rotameric from conformational exchange. Osmolyte perturbation using sucrose affects conformational, but not rotameric exchange, thereby allowing conformational exchange to be observed using X-band EPR.⁴⁰ However, solvent accessible sites are not well suited to this technique because

of the possibility of a false positive.²⁰ A bifunctional spin label (which attaches to two engineered cysteines) or a rotamerically restricted spin label can be used to eliminate the effect of rotameric exchange, but these solutions require costly changes to the experimental protocol.^{29,41} By contrast, saturation-recovery (SR), a pulsed EPR technique, can distinguish between rotameric and conformational equilibrium without the need to perturb the sample.^{35,37} SR allows the measurement of the spin-lattice relaxation time, T_1 , which is related to the nitroxide's spin-lattice relaxation rate, W , by $W = (2T_1)^{-1}$.³⁵ SR experiments monitor the recovery of intensity of the central EPR resonance after a strong saturation pulse, then fit the recovery curve to an exponential equation defined by the magnetization vectors of the system and the implied or effective spin-lattice relaxation time(s).³⁷ If two conformational states are present, two resultant rates will be observed in the presence of varying concentrations of a paramagnetic relaxant, such as oxygen, requiring a double exponential fit and thereby allowing conformational exchange to be distinguished from rotameric exchange.^{35,37}

2.4. Motional model for nitroxide EPR spectral simulation

Multicomponent spectra resulting from conformational exchange are composed of individual component spectra that can be extracted by computational simulation using a model conceived by Freed and coworkers called microscopic-order-macroscopic-disorder (MOMD)^{33,42} and developed into a LabView dock by Christian Altenbach of UCLA. MOMD characterizes the motion of a nitroxide spin label in a three-frame coordinate system, shown graphically in Figure 2.4.1, and can be applied to spectra in the intermediate or slow motional regimes (roughly $1 \text{ ns} < \tau < 30 \text{ ns}$). The magnetic frame (x_M, y_M, z_M) defines the g tensor (the interaction of the paramagnetic electron with the applied magnetic field) and A or hyperfine

tensor (the interaction of the electron with the nucleus). The x_M axis is defined to coincide with the N-O bond, the z_M axis with the N p-orbital, and the y_M axis by the right-hand rule. The magnetic frame is offset from the rotational diffusion frame (x_R, y_R, z_R) by the fixed diffusional tilt angle, β_D .^{30,32} The rotational diffusion frame defines the logarithmic rotational correlation rate tensor, R , which is inversely proportional to the rotational correlation time, and thereby represents the instantaneous motion of the R1 label. The final coordinate frame is the protein director (x_D, y_D, z_D) which is offset from the rotational frame by the angle θ . The protein fixed director is used to define an order parameter which is dependent on the instantaneous change of θ and simulates anisotropy.^{28,33,42}

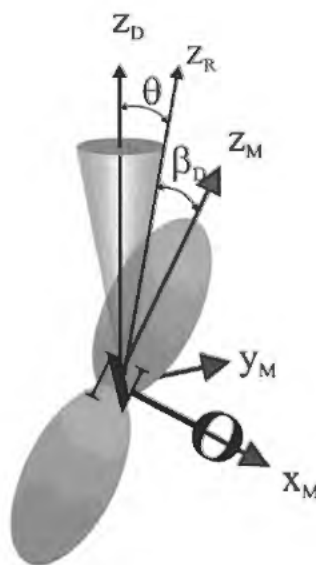


Figure 2.4.1. MOMD slow-intermediate motional simulation model. The motional freedom of R1 is modelled by instantaneous motion of z_R from z_D , fixed with the protein, and offset from the magnetic tensor frame by the fixed angle, β_D . Figure is reproduced.³¹

2.5. Using SDSL-EPR to measure labelling site solvent accessibility

When the power at which a CW EPR spectrum is collected is gradually increased, the intensity of the EPR signal increases with the square root of the applied power, $P^{1/2}$. At high power levels, the population difference between the substates of the paramagnetic electron

erodes because relaxation is slower than the excitation by the microwave power, resulting in a plateau of signal intensity called saturation. Since signal intensity is directly related to the spin-lattice relaxation rate, the presence of paramagnetic reagents (such as O₂) near the nitroxide label confers faster relaxation, thereby increasing the power level required to reach the saturation point. Power saturation EPR experiments extract P_{1/2}, the power at which signal intensity is half the unsaturated sample's intensity. By obtaining P_{1/2} values for a sample under O₂ and N₂ gas, and taking the difference, Δ P_{1/2}, the accessibility of the label to O₂ is found. Since O₂ is nonpolar and preferentially partitions into the lipid membrane, Δ P_{1/2}(O₂) is generally directly proportional to the membrane depth of the label, but must be interpreted with caution especially for spin labels near the membrane-solvent interface.^{19,20}

2.6. Using SDSL-EPR to measure inter-label distances

There are a few ways of using EPR to measure distances in proteins.^{20,21,29} When nitroxide labels are within 20 Å of each other, dipolar coupling between them leads to line broadening and associated reduction in the relative intensity of the central peak of a CW EPR spectrum.⁴³ Because M2 is a tetramer, conventional labelling with MTSSL places four R1 labels on the protein. In a 'dilute-labelled' sample, unlabeled M2 peptide is mixed with labelled M2 at a 4:1 ratio, thereby producing M2 in which each tetramer has one R1 label on average.²⁰ The ratio between the central peak intensity of the dilute-labelled spectrum to the fully-labelled spectrum (in which there are four R1 labels on average) is termed Ω. Since distance dependent dipolar coupling only affects distances less than 20 Å (i.e. intra-tetramer distances), Ω of 1 indicates all distances are greater than 20 Å while Ω of greater than 1 indicates the presence of intra-tetramer distances less than 20 Å.¹⁹ Dipolar coupling distance measurements can be quite accurate,²⁰ but the process of deconvolution of comparison

spectra is not possible for more than two different distances, which are expected in conformational exchange.⁴⁴ For this reason, double-electron-electron-resonance (DEER) is more commonly used to compute distances, but is only accurate for distances between 20 and ~ 60 Å,^{29,41} longer than the distances expected for M2. DEER experiments on the M2 truncation provided some information consistent with published structures in a previous publication of our group,²³ but DEER studies were not undertaken for this work.

Chapter 3. Materials and Methods

3.1. M2FL purification and spin labelling

Full length M2 was overexpressed with single site cysteine mutations in the C-terminal amphipathic and transmembrane helices as described previously.²² The native cysteine C50 at a palmitoylation site was mutated to serine. Each 1 L growth was lysed separately as a ¼ L pellet in 9.5 mL lysis buffer (50 mM Tris pH 8, 40 mM octyl b-D-glucopyranoside (OG), 150 mM NaCl, 0.2 mg/mL DNase I, 0.25 mg/mL lysozyme, and 500 mM AEBSF). The resultant lysed mixture was sonicated for 40 minutes and centrifuged for 30 minutes at 15,000g. The supernatant was incubated for 30 minutes with constant mixing in 1 mL Ni-NTA resin (GoldBio), 20 mM imidazole, and 0.1 mM TCEP. To remove non-M2 proteins, the column was washed with Wash I (50 mM Tris pH 8, 150 mM NaCl, 40 mM OG, 20% v/v glycerol), Wash II (50 mM Tris pH 8, 20 mM OG, 20% v/v glycerol), and Wash III (50 mM Tris pH 8, 4 mM OG, 20% v/v glycerol, 20 mM imidazole). M2 was spin labeled on the Ni column with a 10-fold excess of MTSSL (Toronto Research Chemicals) delivered in acetonitrile at 25 °C with constant mixing for 36-48 hours. The spin labeling buffer was then eluted and the column washed in 5 mL Wash III for 20 min. with constant mixing. His-tagged M2 protein was eluted with two washes of 5 mL of elution buffer (50 mM Tris, 300 mM imidazole, 4 mM OG, and 20% v/v glycerol). Sodium dodecyl sulfate polyacrylamide gel electrophoresis (SDS-PAGE) confirmed presence of purified M2 protein.

3.2. Selection of lipid mixes and detergent mediated reconstitution

M2 protein obtained in a single purification was independently reconstituted into lipid environments incorporating 1,2-dioleoyl-sn-glycero-3-phosphoethanolamine (DOPE), 1,2-dioleoyl-sn-glycero-3-phosphocholine (DOPC), and 1,2-dioleoyl-sn-glycero-3-phospho-L-

serine (DOPS), shown in Figure 3.2.1. The lipid environments were chosen because of their use in a small angle X-ray scattering study of M2 membrane curvature generation^{18,45} (section 4.1). These vesicles were composed of 4:1 DOPE:DOPS and 4:1 DOPC:DOPS. To study the effect of cholesterol, 30 mol% was added to form separate liposomes of 56:14:30 DOPE:DOPS:Cholesterol and DOPC:DOPS:Cholesterol. DOPE and DOPS were obtained in chloroform and DOPC was obtained as powder and dissolved in chloroform (Avanti Polar Lipids). Chloroform was removed under a stream of nitrogen and lipid films were dried under high vacuum for 12 h. Lipid films were re-suspended in extruder buffer (50 mM Tris pH 8, 100 mM KCl, 1 mM EDTA) at a total lipid concentration of 9.36 mg/mL and alternately sonicated and vortexed. The lipid films were extruded 15 times through a 20 µm filter using an Avanti Mini-Extruder. Each lipid suspension was solubilized in 40 mM octyl-glucopyranoside (OG) and equilibrated for 30 min. M2 protein was added to the lipid film to achieve a protein:lipid ratio of 1:40¹⁸. For dilute labelled samples (section 2.6), unlabeled peptide was added at a 4:1 ratio with the total amount of added M2. The mixture was diluted in extruder buffer to obtain an OG concentration of 15 mM. Six 50 µL aliquots of a slurry of hydrophobic polystyrene beads (BioBeads SM-2, Bio-Rad) degassed for 1 h. in 50 mM Tris pH 8, 100 mM NaCl were added in 15 min. increments at 4 °C to the protein-lipid suspension with constant mixing. After removing Bio-Beads, the proteoliposomes were pelleted at 313,000 g for 1h. using an Optima-MAX-TL ultracentrifuge (Beckman-Coulter). Pellets were re-suspended in 200 µL of supernatant and re-pelleted using the same ultracentrifuge configuration.

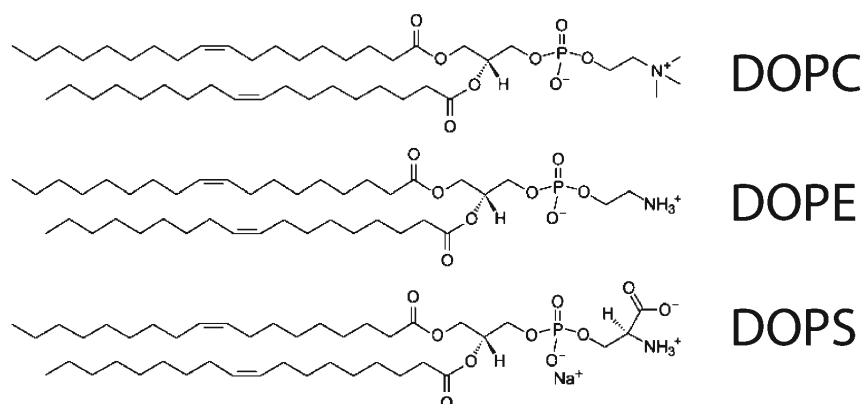


Figure 3.2.1. Structures of lipids used in this thesis.

3.3. CW and power saturation EPR collection

Samples used for EPR spectroscopy were prepared from re-suspended pellets and loaded into gas permeable TPX capillary tubes. Continuous wave (CW) EPR spectra were collected on a Bruker EMX X-band EPR spectrometer with an ER4123D resonator at room temperature. For analysis of spectral line shapes, spectra were collected at 2 mW incident microwave power, 1 G field modulation at 100 kHz amplitude, and 150 G sweep width. Line shapes used for comparison of lipid environments were doubly integrated and normalized to the same number of spins. Power saturation data were collected twice for each lipid environment: once in ambient air, and once under a gentle stream of nitrogen gas. The former were collected using 19 power levels and the latter were collected using 8 power levels (Appendix C).

3.4. EPR analysis and spectral simulation

Dilute labelled CW EPR spectra were normalized as described in section 3.3 and simulated in the slow-intermediate motion MOMD model using 'Multicomponent,' a LabView dock developed by Christian Altenbach. A (hyperfine), g (Zeeman), and R (logarithmic rotational correlation rate) tensors were varied between labelling sites, but were constant for a given labelling site in all lipid environments (L43R1 was fit using slightly different parameters

between the wildtype and penta-Ala constructs). The values for the A and g tensors are usually constant for R1 labels attached to membrane proteins: starting values of $A = (5.1, 5.3, 34.3)$ and $g = (2.0084, 2.0058, 2.0020)$ were used^{30,32}. However, A tensors in particular can vary depending on local polarity and membrane accessibility⁴⁶, so A tensors were allowed to vary between components. Only A and R tensors varied between the two simulated components, and among lipid treatments of the same labelling mutant, only the populations of the components varied. All fits using the MOMD model solve the stochastic-Liouville equations using the Levenberg-Marquardt fitting strategy. Floating variables were limited to a maximum of 20,000 iterations and the step size for A and g tensors was restricted to 10^{-8} and 10^{-11} , respectively. Maximum variations were 0.6 G for A and 0.001 G for g. The W tensor (Lorentzian line width) was not varied. Along with R tensors for the two components, refinement can include changing the diffusional tilt angles ($\alpha_b, \beta_b, \gamma_b$). Because M2 is axially symmetrical, only β_b significantly affects the simulation and was restricted to 90° to simulate X-axis anisotropy while α_b and γ_b were restricted to 0° . Fitting parameters are listed in Appendix B.

Chapter 4. Lipid Intrinsic Curvature Propensity Affects Conformational Exchange in Full-Length M2

4.1. Background: Role of lipids in generation of membrane curvature

Lipids are widely recognized as filling a crucial role in the generation of membrane curvature, a key requirement for viral budding and scission, and the interaction between membrane proteins and lipids is an active area of research.^{47,48} The intrinsic curvature of a biological membrane (curvature without protein interactions) is determined by the molecular packing of lipids it consists of.⁴⁸ For instance, PC lipids (with methylated head groups) are roughly cylindrical and form membranes with zero spontaneous curvature, whereas PE lipids (with smaller head groups) favor formation of intrinsically curved membranes.^{45,49,50} The curvature properties of membranes can be defined easily: at any point on a curved membrane, a normal flat surface can be extended and the principle curvatures, c_1 and c_2 , defined as the reciprocals of the radii that define a circle which includes the curved membrane. To a simple approximation, the mean curvature is the average of the two curvatures, while the Gaussian curvature is the product. As a result, a flat membrane has zero mean curvature and zero Gaussian curvature; rolling the membrane can only change mean curvature and the Gaussian curvature is altered only by stretching, compression, or tearing.⁵¹ Flat membranes with zero curvature exist in the lamellar phase, L_α , while an increase in Gaussian curvature results in the inverted hexagonal phase, H_{II} . The inverted cubic bicontinuous phase (Q_{II}) has three low energy surfaces defined by the space groups $Pn3m$, $Im3m$, and $Ia3d$ (commonly referred to as gyroid).^{48,51} These surfaces are unique because they possess bicontinuous negative Gaussian curvature⁵² (occasionally called saddle-splay curvature), the type of curvature necessary for membrane scission.^{48,49,51-53}

4.2. Introduction: Lipid intrinsic curvature is related to M2 budding function

Small angle X-ray scattering (SAXS) results were recently reported showing that the full-length M2 protein generates cubic bicontinuous phase lipid membranes in lipid mixtures comprising elevated DOPE concentration.¹⁸ Since DOPE and DOPC are approximately the same size and differ only in intrinsic curvature propensity, a ternary mixture (along with DOPS, which alters membrane charge) is frequently used to vary membrane curvature *in vitro*.^{45,50} At a variety of peptide:lipid ratios, membranes with >60 mol% DOPE were characterized in a number of cubic lipid phases. In particular, the *Ia3d* gyroid phase was isolated at a peptide:lipid ratio of 1:40 for the full-length protein in an 80 mol% DOPE membrane. Additionally, the AH construct, which contains no transmembrane helices and only the 47-61 residues of the amphipathic helix, generated cubic phase in an increased variety of lipid environments, including those with 0 mol% DOPE, providing evidence that curvature generation by M2 is accomplished by the amphipathic helix. By contrast, the penta-Ala mutant construct generated cubic phase at a reduced number of lipid environments.¹⁸

To characterize the effect of membrane curvature on M2's conformational dynamics, full-length M2 was reconstituted into 80:0:20 DOPE:DOPC:DOPS and 0:80:20 DOPE:DOPC:DOPS liposomes at a constant 1:40 peptide:lipid ratio. Under these conditions, SAXS data showed the presence of isolated cubic and lamellar phase, respectively.

4.2. CW EPR lineshapes are multicomponent, revealing the presence of two conformations whose populations depend on lipid composition

Figure 4.3.1 shows the CW EPR spectra of full-length M2 protein labelled at five selected sites (shown in Figure 1.2.1) reconstituted into 80:20 DOPE:DOPS (cubic phase) and 80:20 DOPC:DOPS (lamellar phase) LUVs.

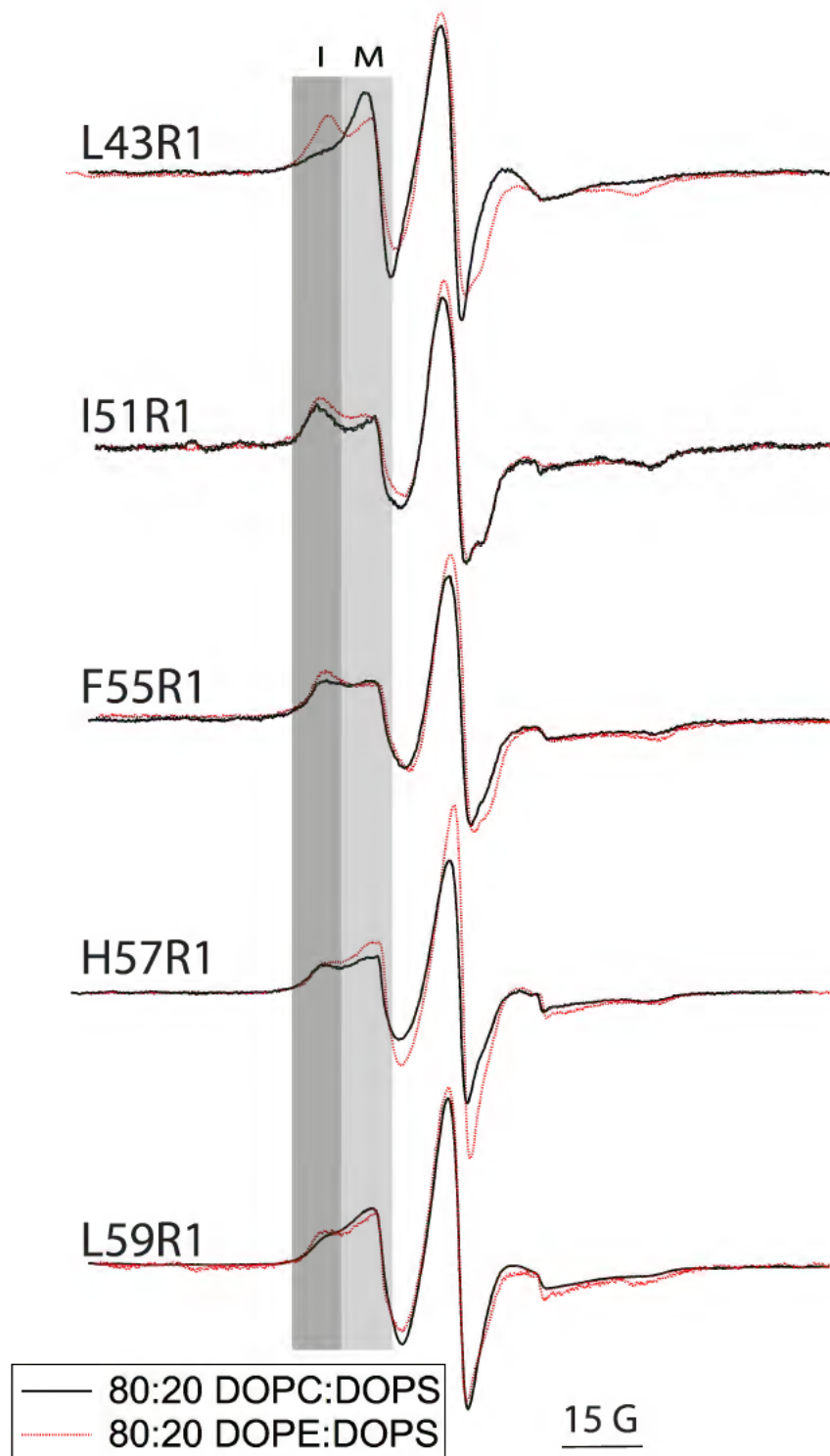


Figure 4.3.1. Multicomponent CW EPR spectra of M2FL at selected labelling sites. ‘I’ refers to the immobile component; ‘M’ refers to the mobile component. 80:20 DOPE:DOPS lipids produce a cubic phase membrane, while 80:20 DOPC:DOPS lipids produce lamellar.

The multicomponent nature of the spectra can be seen visually by the 'two-hump' nature of the low field peak. Because the broader spectral component is immobilized relative to the other component, it is referred to as the immobile component, **I**, to contrast with the mobile component, **M**. Variation of the lipid environment causes variation in the population of the spectral components, as evidenced by a change in the intensity of the two positions of the low field peak. However, both components are present in all spectra, meaning that the shift in populations characterizes a dynamic equilibrium between two states. The immobile component is more populated in the cubic lipid environment (80% DOPE) than it is in the lamellar lipid environment (80% DOPC) for all sites except H57, and the difference is largest for site L43. As mentioned in section 2.3, multicomponent spectra can result from conformational or rotameric exchange. To determine the nature of the exchange event, saturation recovery (SR) EPR was conducted by Dr. Jimmy Feix at the National Biomedical EPR Center, Medical College of Wisconsin on selected labelled samples. Preliminary data available at the time of writing confirms the multicomponent result is from conformational exchange, consistent with findings from previous studies of the Howard Group.²³

The difference in CW lineshape between the labelled sites is a result of a difference in spin label mobility. The central amphipathic helix sites I51R1 and F55R1 display significant immobilization of the spin label in both lipid environments, compared with L43R1 (in the transmembrane helix) and L59R1 (at the end of the amphipathic helix). Indeed, previous EPR experiments have shown I51 and F55 to be located on the membrane or hydrophobic side of the helix²², accounting for the reduced motion of the spin label positioned at those sites. The H57R1 label experiences greater mobility than the central amphipathic helix sites and does not experience the lipid dependent lineshape change described above, most likely

because of its position on the hydrophilic side of the helix and exposed to solvent. The large change in mobility associated with lipid environment observed for L43R1 indicates that this residue engages in a significant change in mobility between the two states. By contrast, the change in mobility is much less significant for the amphipathic helix sites, but the changes in lineshape suggest that the entire amphipathic helix experiences a concerted change in mobility during conformational exchange.

Further qualitative characterization of the equilibrium between the mobile and immobile components can be accomplished by calculation of the inverse central peak width, ΔH^{-1} , shown in Figure 4.3.2. Because immobilization contributes to spectral broadening, a smaller ΔH^{-1} indicates less mobility.^{19,20} This general trend is consistent with greater immobilization in cubic phase membranes versus lamellar phase. However, the difference in width is small between treatments due to the fact that both components contribute to the central peak, and thus the difference in inverse widths is not always significant. More accurate determination of the nature of the conformational equilibrium can be accomplished by spectral simulation.

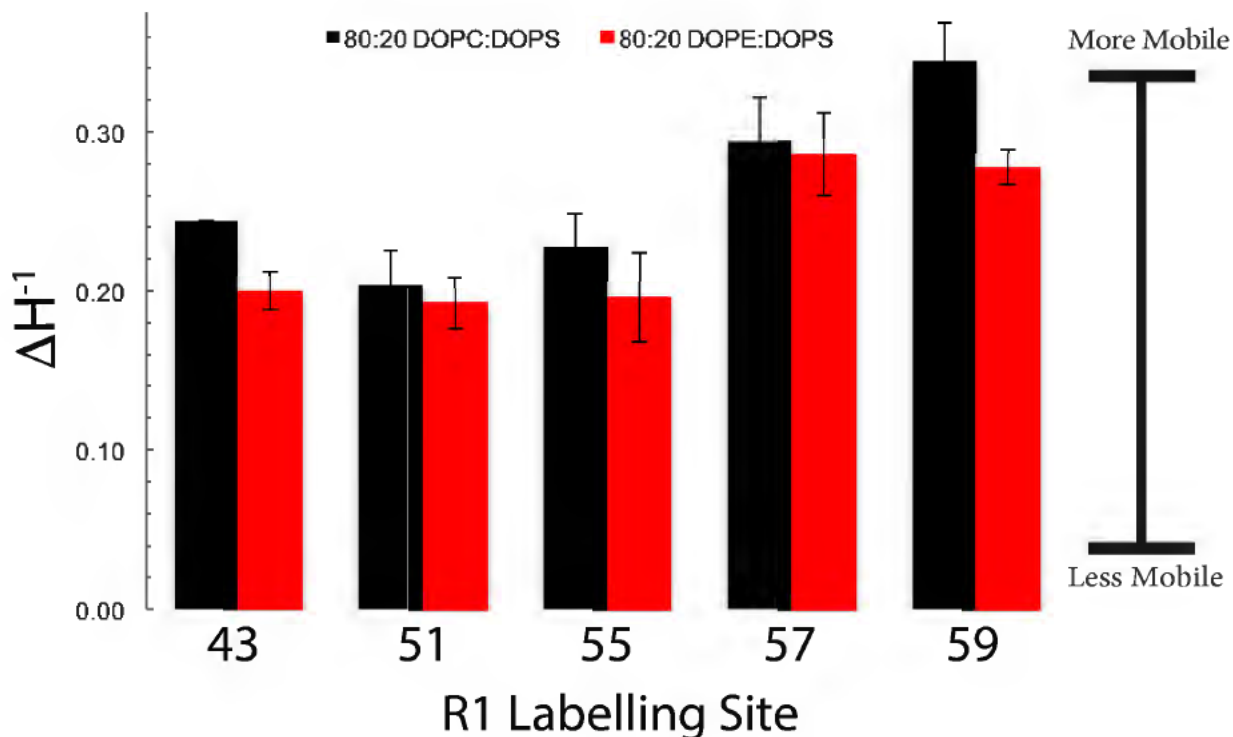


Figure 4.3.2. Inverse central peak width, ΔH^{-1} , a qualitative characterization of mobility for the five labelled sites in cubic (PE) versus lamellar (PC) phase lipid environments.

Equilibrium between the mobile and immobile states can be modelled by computational simulation of multicomponent spectra and extraction of the individual components under the assumption that they are the same between two lipid treatments, but are present in different quantities in each spectrum. The simulation of M2FL spectra was accomplished by fitting with ‘Multicomponent’, a LabView program written by Christian Altenbach that uses the MOMD model³³ (section 2.4). Simulations of multicomponent EPR spectra for five labelled sites are shown in Figure 4.3.3. Multicomponent simulation is complicated by the fact that a single component can often not be isolated experimentally, usually requiring spectral subtraction. However, simulations of the EPR spectra in cubic and lamellar lipid environments achieved consistently reproducible fits, providing confidence that

the fitting parameters appropriately modelled the motion of the spin label without the need for an isolated spectral component.

For spectra of L43R1, consistently reproducible fits required a compromise between fitting the central peak or the low and high field peak to obtain reasonable simulations. The results from fitting the low and high field peaks are shown here even though the central peak deviates significantly from the simulated spectra. There are a few possible explanations for the deviation: first, L43 could experience a conformational change in which the spin label's motion is either not X-axis anisotropic or is immobilized by the transmembrane helical bundle so significantly that both components have high correlation times. To a first approximation, fits could not be improved by accounting for these possibilities. More likely, L43R1 experiences an interaction with the membrane that affects its lineshape in a way that cannot be easily accounted for by the limited computational intensity used in the MOMD model^{42,46}. Another possibility is that L43R1 interacts with the membrane differently from the other labelling sites and requires a substantially different simulation treatment. For example, the A tensor is known to be strongly dependent on membrane interactions.⁴⁶ The caution in interpretation of the L43R1 spectral simulations should not, however, limit interpretation of the lineshapes themselves. While it is clear that L43 is a significantly immobilized site, the true nature of the conformational change in this region would require additional labelling sites to elucidate.



Figure 4.3.3. Spectral simulations (red) of dilute labelled CW EPR spectra (black) for five selected labelling sites in cubic (PE) and lamellar phase (PC) lipid environments. Percent of immobile component population is listed to the right.

Simulations using the MOMD model also enable extraction of the purely mobile and purely immobile components for each spin labelled mutant, shown in Figure 4.3.4. Because the magnetic tensors vary only slightly between labelling sites and the R tensors are largely consistent between spectra of the same lipid environment, the simulated theoretical spectral components are similar between sites and only differ based on the intrinsic mobility of the part of protein where the spin label is attached. The correlation times for the mobile components range from 2.12 - 4.93 ns while those for the immobile component range from 7.07 - 9.90 ns. Interestingly, the both the mobile and immobile components of L43R1 are characterized by the highest mobility of all the sites' respective components. As part of the hinge region between the TM and amphipathic helices, site 43 may experience more mobility than the purely amphipathic helical labelling sites, but this result is more likely an artifact of the compromises made during the simulation procedure for this site (note the discrepancy between the central line amplitudes of the simulated and actual spectra in Figure 4.3.3 and the discussion above). The difference between lineshapes of the spectra of these sites is somewhat dependent on the intrinsic mobility of the spin label. The I51R1 and F55R1 spectra contain highly immobilized immobile components due to the restricted motion of the spin label attached to a secondary structure element, in this case the amphipathic helix. By contrast, the spectrum of L59R1 features a less pronounced immobile component, suggesting decreased rigidity as the helix ends and the chain becomes unstructured.

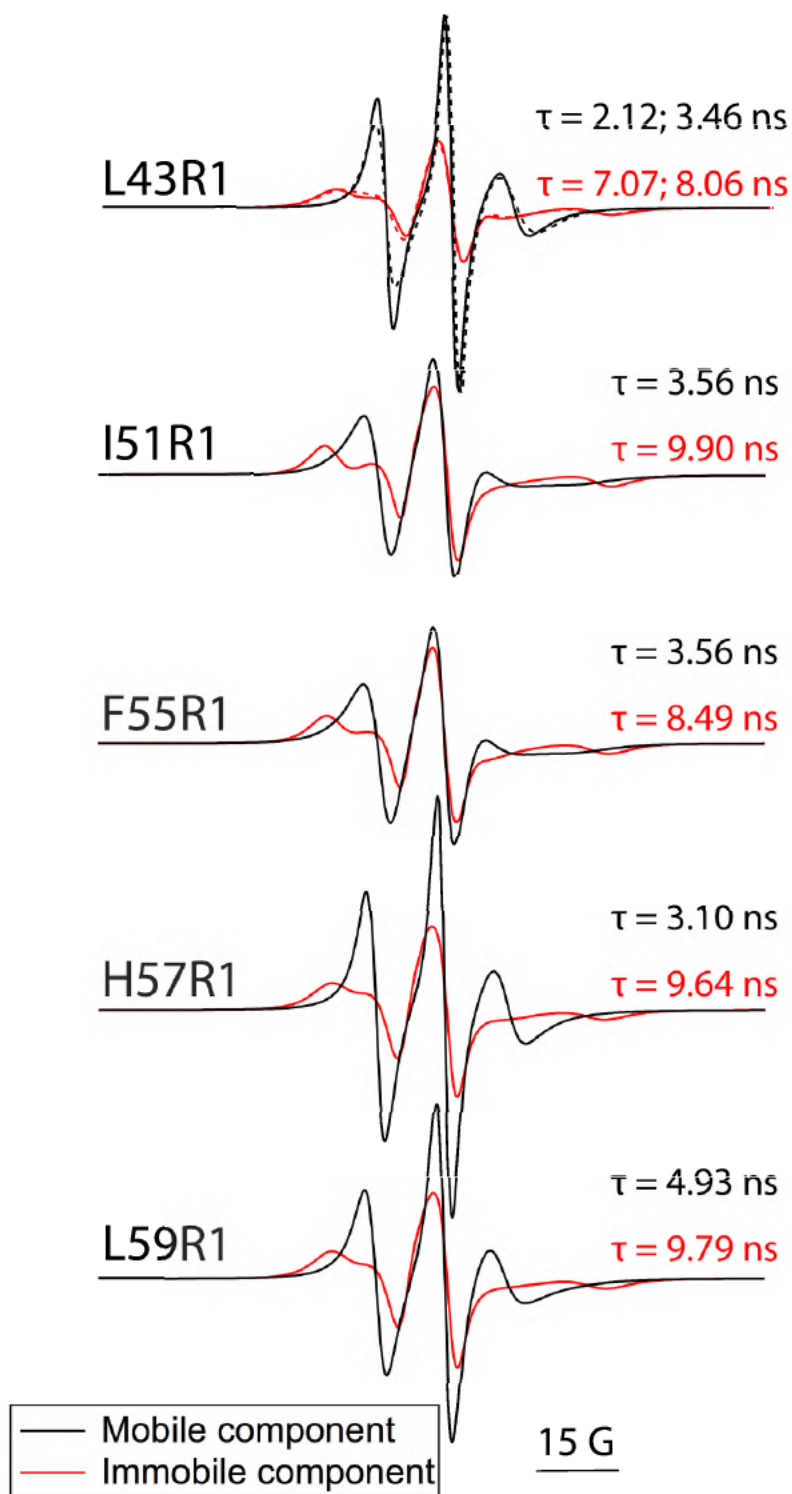


Figure 4.3.4. Extracted mobile and immobile components. Correlation times extracted using the MOMD model for the mobile (black) and immobile (red) components are listed on the right along with the isolated component spectra for each labelled site. Dotted lines for L43R1 result from slight modifications for the 5Aa construct (discussed later in Chapter 6).

4.4. Curvature promoted conformation features a more tightly packed and shallower AH

Power saturation EPR provides information about the depth of a particular spin label in the lipid membrane (section 2.5). The results of oxygen power saturation experiments for five selected labelled mutants are shown in Figure 4.4.1. A large $\Delta P_{1/2}(O_2)$ indicates a more buried spin label^{19,20}. With the exception of L43R1, which is located in the transmembrane domain, the amphipathic helix residues become less buried in the cubic phase membrane than in lamellar phase. The opposite change for H57R1 may be explained by the fact that it is on the water-exposed side of the helix as opposed to I51, F55, an L59 which face the membrane. If the helix rotates around its long axis (parallel to the membrane surface) as part of the conformational change, the sides of the helix may experience opposite changes in solvent accessibility. These results suggest the immobile conformation of M2 possesses a shallower amphipathic helix than the mobile conformation.

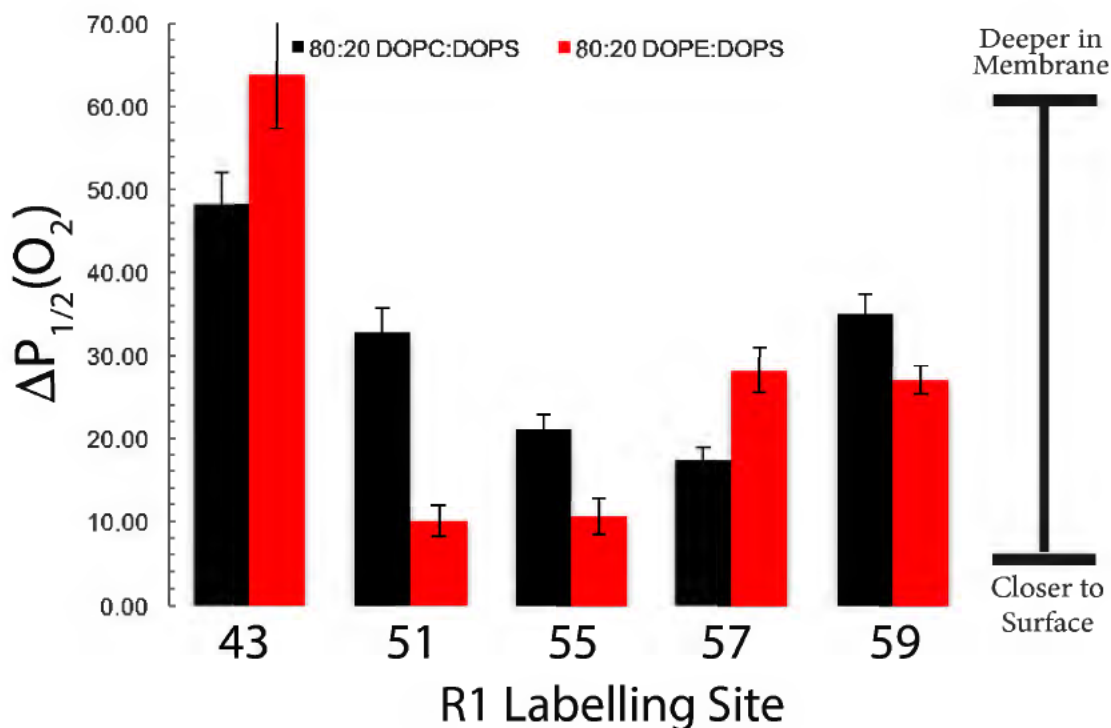


Figure 4.4.1. Oxygen power saturation for five selected labelled mutants. Samples have on average four spin labels per tetramer (fully labelled).

The values of Ω for four selected sites in cubic and lamellar phase promoting lipids are shown in Figure 4.4.2. The fully labelled lineshapes for the four selected sites are shown along with their corresponding dilute labelled lineshapes in Appendix C.

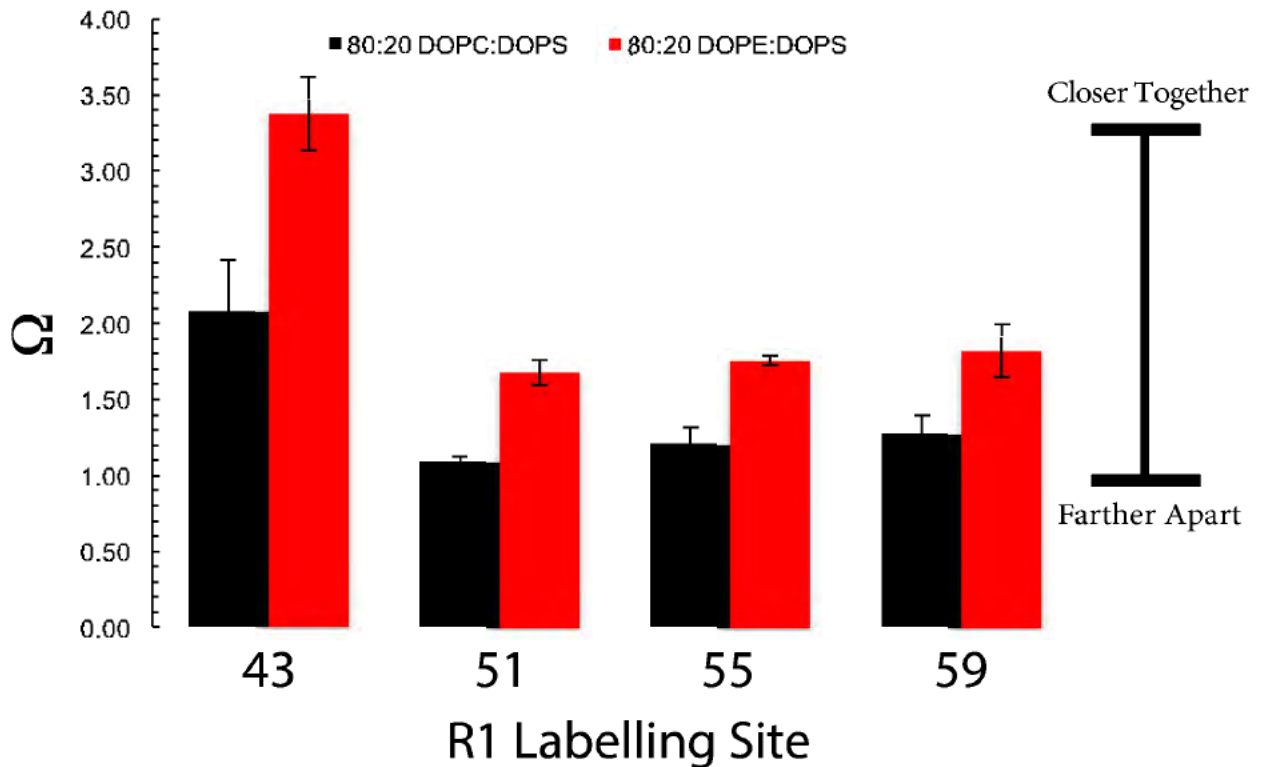


Figure 4.4.2. The ratio between dilute and fully labelled spectral intensities at the central peak, Ω , is a characterization of the distance dependent dipolar coupling between spin labels in the M2FL tetramer (see section 2.6).

The Ω values for M2FLR1 differ depending on lipid environment. The lamellar phase promoting lipids result in Ω values close to 1 for the labelling sites in the amphipathic helix and approximately 2 for L43R1. For all mutants, the cubic phase promoting lipid environment causes an increase in Ω , indicating that the inter-label distance decreases. The shorter distances indicated by the Ω for L43R1 are due to the transmembrane helices being closer together than the amphipathic helices. The combined results suggest the M2 tetramer's

helices become more closely packed in the immobile conformation, relative to the mobile conformation.

4.5. Curvature results from interplay between M2 and membrane dynamics

These results demonstrate a lipid-dependent conformational change in full-length M2 that is associated with curvature propensity of lipids. The impact of lipid composition on membrane protein conformational dynamics has been observed in a number of systems.⁵⁴ In particular, the intrinsic curvature propensities of lipids is believed to play a crucial role in the generation of membrane curvature by integral membrane proteins.^{47,55} DOPE and other PE lipids possess unmethylated head groups, which are small and cause membrane packing defects or curvature.⁴⁸ PE lipids have been copurified with membrane proteins, suggesting a close relationship between the protein and the identity of the nearest neighbor lipids. Additionally, several membrane proteins that require PE lipids to access a functionally-relevant conformation have been identified.⁵⁶ For example, the active transporter lactose permease (LacY) requires PE for proper orientation in the membrane.⁵⁷ Addition or depletion of PE modulates a dramatic conformational change that sees the topology of the protein substantially reversed.⁵⁸

The phase behavior of the DOPC:DOPS and DOPE:DOPS lipid systems used in this study have been extensively characterized by the groups of Tilcock and Cullis, who developed the theories of lipid membrane polymorphism, in which a variety of structures can be accessed by model membranes and transferred to membrane proteins.^{59,60} While DOPE has been shown to form H_{II} phase by NMR⁶¹ and SAXS⁵⁰, X-ray diffraction phase data suggested PE systems require stabilizing compounds such as tetradecane to achieve H_{II} phase and instead adopt lamellar phase like PC lipids.⁴⁵ The role of PS lipids is also as a membrane

stabilizer, but is dictated by their charge: mixtures of DOPC or DOPE with DOPS display a remarkable sensitivity to divalent cations or pH in which even low mol% DOPS induces highly stable lamellar phase in mixtures with PE and PC. In the presence of Ca^{2+} or pH below 5.5, phase separation occurs thereby allowing formation of isolated H_{II} or lamellar phase by PE or PC, respectively. In short, DOPS modulates lipid polymorphism based on pH and charge.⁶²⁻⁶⁵

The dual conformation system identified here is remarkably similar to results observed previously for the impact of cholesterol on M2 conformation. Increasing bilayer thickness was found to promote population of a conformation with a tightly packed helical bundle.²⁶ A conformational exchange model for the M2TMC construct confirmed this result and showed that M2 conformation is dependent on membrane composition.²⁴ In this same construct, cholesterol-dependent conformational exchange was demonstrated in which cholesterol stabilized an immobile conformation with shallower amphipathic helices;²³ cholesterol-dependent conformational change is studied in greater detail in Chapter 5. Conformational plasticity in M2's TM region has been demonstrated to explain the protein's pH-dependent ion channel activity and this same conformational freedom may be related to curvature inducing functionality of the amphipathic helices.⁶⁶⁻⁷⁰ In particular, the M2TM region has been shown to access an immobilized state in a viral mimetic membrane.⁷⁰ This result is consistent with the observed immobilization of the TM helix labelling site, L43R1, in the cubic phase membrane since the viral mimetic mimics high curvature regions near the viral budzone.^{15,17,70} Additionally, the finding that the M2 TM and amphipathic helices become more tightly packed in the cubic lipid phase is consistent with the open/closed conformational exchange that enables M2's ion channel activity. MD simulations have

modelled the open and closed channel states, suggesting that a more tightly packed tetramer corresponds to the closed channel state.⁷¹ Indeed, our group identified conformational exchange in M2TMC by SDSL-EPR in which the deactivated (closed) channel state stabilized by pH 7.8 corresponds to a conformation that features shallower and more closely packed amphipathic helices than the open channel state (at low pH).²⁵ Presumably, the conformational change of the TM and amphipathic helices is concerted; that is, tight packing of the TM region by pH change causes a conformational change in the amphipathic helices. Similar conformational exchange has also been observed by solid-state NMR.⁶⁶ In a viral mimetic membrane, high pH favors more tightly packed TM helices, while low pH stabilizes a loosely packed state in which the channel is open. By contrast, PC membranes can stabilize the loosely packed state even at high pH.⁶⁶ Since all the work in this thesis was conducted at high pH (7.8), the observation that PE lipids stabilize a more tightly packed conformation is consistent with the existing dual-conformation model for M2's proton channel activity.

Conformational exchange in M2's amphipathic helix has also been shown to be pH-dependent by SDSL-EPR²⁵. The similarity between the immobilized, tightly packed conformations observed at high pH and in cubic phase membranes in this thesis is consistent with the existence of concerted conformational exchange in M2's amphipathic helices that is modulated by pH or membrane dynamics. In particular, the observation that isolated budding-relevant cubic phase membranes stabilize the immobile conformation supports the hypothesis that the immobile conformation generates curvature for viral budding. By extension, the analogous high pH closed-channel conformation is hypothesized to be similar to the non-budding, mobile conformation stabilized by the zero curvature lamellar phase membrane. Solid state NMR has been used by the Hong Group to investigate membrane

curvature and protein structure simultaneously for M2TMC. M2(21-61), containing both the TM and amphipathic helices, was capable of generating high curvature membrane phases in both viral mimetic and PC based membranes, but M2(21-46), containing only the TM domain, was incapable of this curvature induction. Additionally, generation of high membrane curvature was associated with weak binding of the channel-blocking drug amantadine, indicating that the high curvature stabilized state featured a closed channel.⁶⁷ These results and those described in this thesis are consistent with a curvature generation function for M2's amphipathic helix and suggest that the pH-dependent ion channel and curvature induction functions are largely independent of each other. The non-budding, immobile conformation observed in PC membranes in this study (at high pH) is almost certainly not the same as the open channel conformation even though the lower TM region and amphipathic helices share similar properties.

These results in conjunction with NMR results described above suggest that the budding and non-budding conformations observed here both feature a closed channel, but that the low pH open-channel conformation has a lower TM region and amphipathic helices structurally similar to those in the non-budding, immobile conformation. Further study of the relationship between the pH-dependent TM region and curvature induction amphipathic helix conformational changes may explain whether the TM region plays any role in curvature generation. Hong and coworkers found generation of high curvature possible cubic phase by M2TM+AH, but not M2TM alone,^{67,72} while Pan and coworkers' solution AFM results suggested that M2TM alone may have a role in enhancing curvature generation.⁷³ Interestingly, the conformational link between M2's channel and curvature induction functions may be modulated by membrane changes. In zero curvature membranes, low pH

would activate the proton channel, abolishing curvature induction and allowing M2 to act exclusively as an open channel. By contrast, in the PE-enriched intrinsically curved membrane, low pH promotes increased intrinsic membrane curvature, thereby maintaining curvature generation function.⁶³

The conformational change observed for the amphipathic helix labelling sites in full-length M2 reported here suggest the helix's curvature generation function is accomplished by the immobile conformation, explaining its greater population in cubic phase membranes. The conformational change in the amphipathic helices may also affect the TM domain. Tighter packing of the amphipathic helices during curvature induction likely transfers to the TM domain (or potentially vice versa), thereby accounting for the tightly packed closed channel TM conformation during curvature generation and the disagreement over whether the TM domain is able to generate curvature by itself. In summary, these results support the notion that curvature generation by M2 relies on interplay between the membrane's composition-dependent phase and M2's amphipathic helices. Further characterization of changes to membrane dynamics by cholesterol enrichment is discussed in Chapter 5 and characterization of the effect of the amphipathic helices is discussed in Chapter 6.

Chapter 5. Cholesterol Modulates Lipid Dependent Conformational Exchange in Full-Length M2

5.1. M2TMC cholesterol dependent conformational exchange in POPC:POPG

Previous work by the Howard Group has extensively characterized the effect of cholesterol enriched lipid membranes on the EPR lineshape of M2TMC, but not M2FL²³⁻²⁶. Gradual enrichment of 80:20 POPC:POPG liposomes with cholesterol was shown to promote population of an immobile conformation, with 30% cholesterol lipid environments resulting in lineshapes indicating approximately two-thirds population of the immobile conformation. In addition, cholesterol was shown to promote population of a conformation in which the M2 tetramer was more tightly packed by obtaining inter-label distances using DEER EPR.²³ The cholesterol-dependent conformational equilibrium was observed using a protein truncation rather than the full-length protein.^{22,23} Thus it is unclear whether the observed impact of cholesterol is an artifact of the truncation. To investigate the effect of cholesterol on full-length M2 and the relationship between cholesterol and the demonstrated effect of intrinsic lipid curvature (Chapter 4), several different M2FL, labelled at different sites (Figure 1.2.1), were reconstituted into membranes while varying lipid phase and cholesterol simultaneously.

5.2. Cholesterol modulates curvature dependent conformational exchange

The additional effect of cholesterol was studied for three selected sites, L43R1 (at the end of the transmembrane helix); and H57R1 and L59R1 (representing the amphipathic helix).

Figure 5.2.1 shows the comparison of the effect of cholesterol versus lipid phase on the CW EPR lineshapes of M2FLR1. The lineshapes for L43R1 and L59R1 are characterized by immobilization due to lipid phase (as discussed in Chapter 4, H57 does not show significant lineshape change). Cholesterol enrichment only has a substantial effect on lineshape for the

transmembrane labelling site, L43R1. Both the DOPE and DOPC enriched membranes result in greater population of the immobile component of L43R1 upon addition of 30% cholesterol, as shown in Figure 5.2.2. While cholesterol may be responsible for a small change for the amphipathic helix labelling sites lineshapes, as in Chapter 4 the most significant conformational change detected using these labelling sites appears to take place away from the amphipathic helix itself. In addition to the dramatic change in lineshape observed for L43R1 when lipid phase is altered, this region of the protein experiences a similarly large change when the membrane is enriched with cholesterol. In addition, the similarity of the lineshape for this site in cubic phase and in cholesterol enriched lamellar phase suggests that the addition of DOPE or cholesterol results in similar conformational exchange.

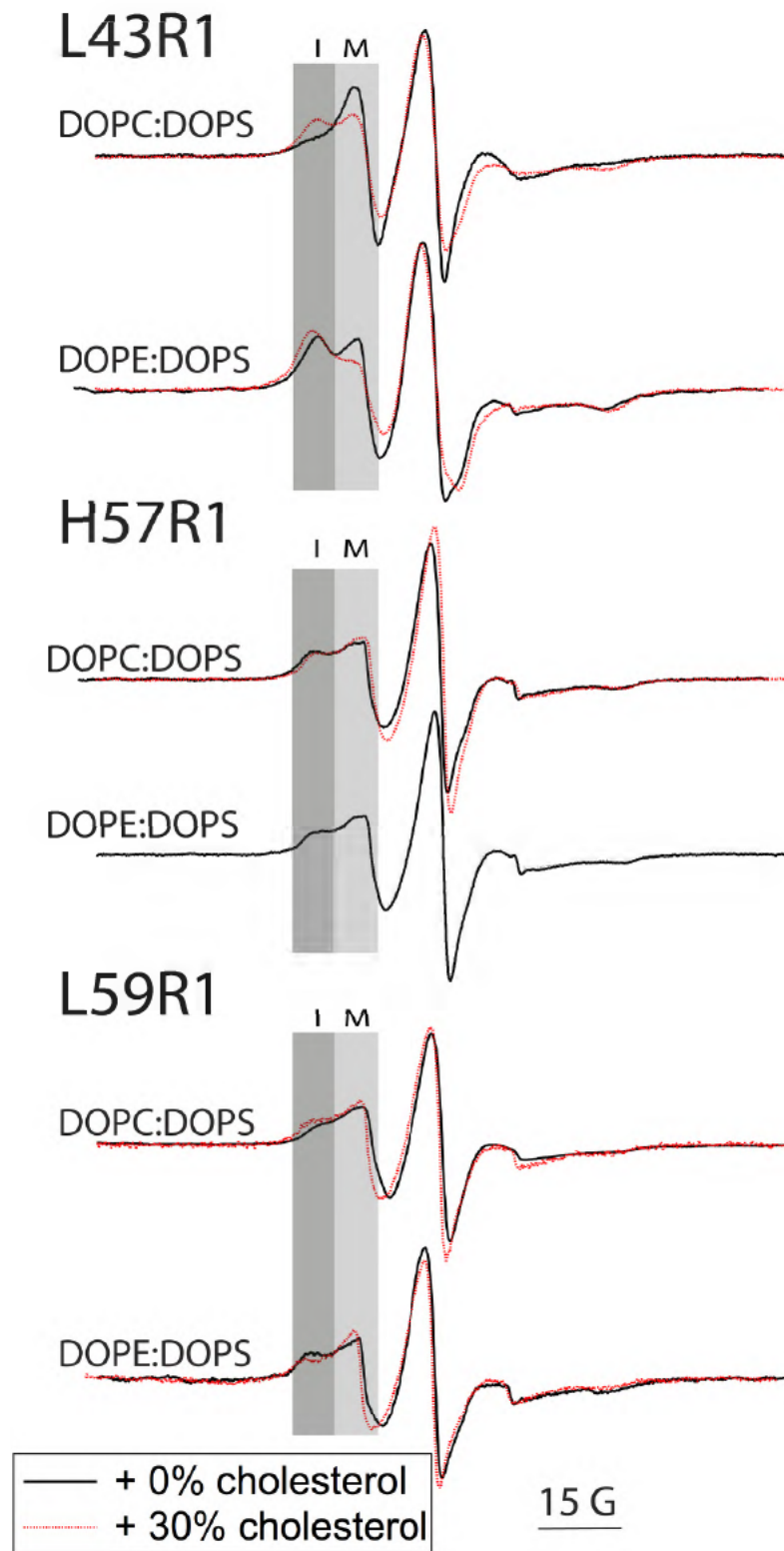


Figure 5.2.1. CW EPR lineshapes of three selected sites varying lipid environment and cholesterol enrichment. 56:14:30 DOPE:DOPS:Chol. and DOPC:DOPS:Chol. are cubic and lamellar phase promoting lipid mixes, respectively, enriched with 30% cholesterol. The difference between fully and dilute labelled spectra is discussed in section 2.6.

As in Chapter 4, simulations using the MOMD model were used to extract the populations of the isolated mobile and immobile components, corresponding to the two conformations of M2. As discussed earlier, the conformational change at L43 is substantial: while the conformations are approximately equally populated in the lamellar phase membrane, the immobile conformation becomes more highly populated with either enrichment with cholesterol or a change to cubic phase (note the similarity between the DOPE:DOPS and DOPC:DOPS + chol. simulations). At the time of writing, proteoliposomes for H57R1 were not available for both of the cholesterol treatments, so simulations are not reported for that mutant. For L59R1, simulations indicate the presence of a small conformational change due to change of membrane phase in which the immobile conformation is stabilized by the high curvature cubic phase generated by DOPE. This observation is the same as that discussed in section 4.4. By contrast, there is no observed change in conformation at this site due to enrichment with cholesterol. Cholesterol therefore has a region specific effect on the conformational dynamics of M2.

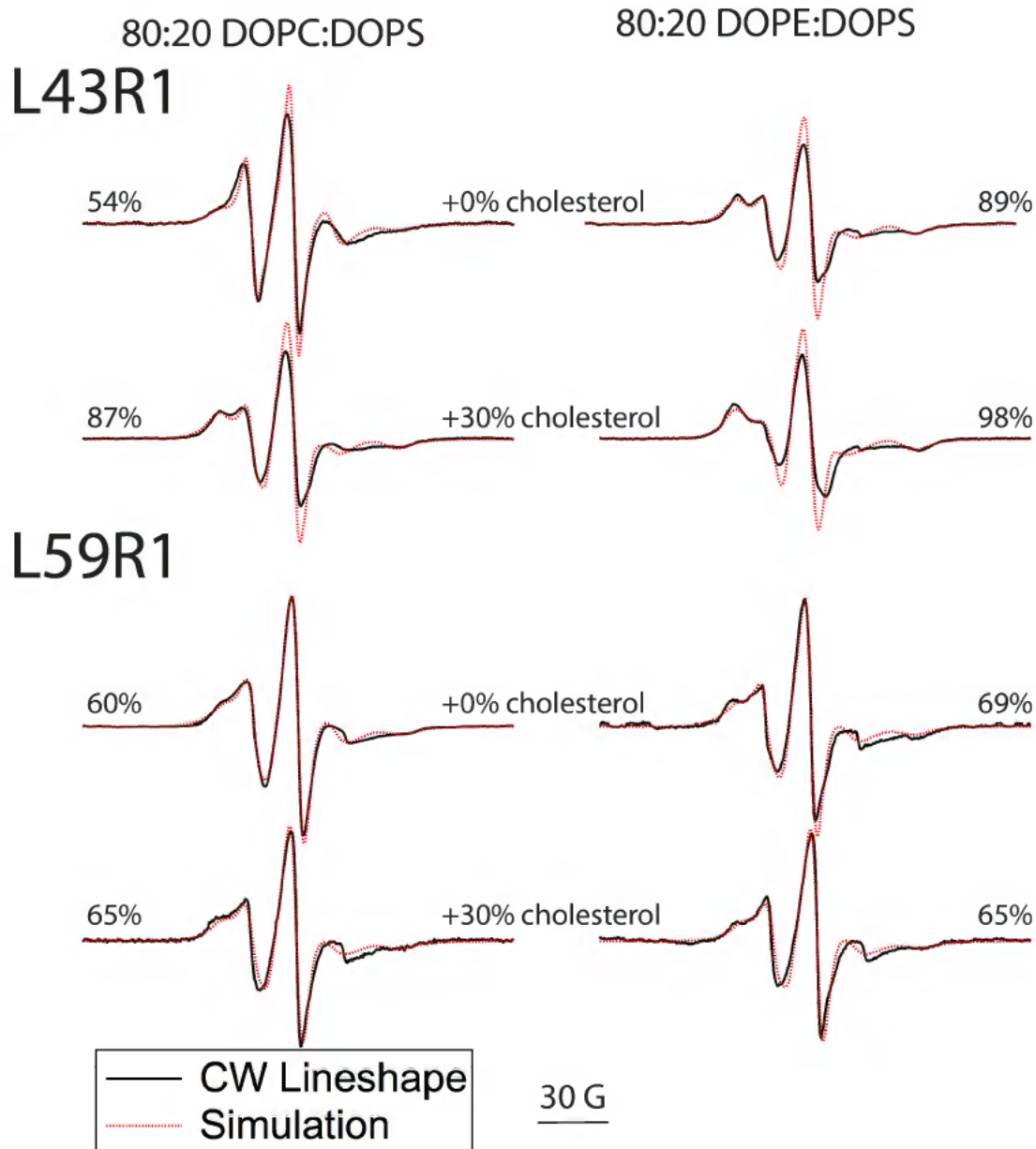


Figure 5.2.2. Spectral simulations (red) of dilute labelled CW EPR spectra (black) for two selected labelling sites in lamellar (PC, left) and cubic phase (PE, right) lipid environments with and without 30% cholesterol. Percent of immobile component population is listed to the left and right.

5.3. Cholesterol-dependent membrane changes at the influenza budzone affecting M2

These results raise the question of whether a cholesterol-dependent conformational change is experienced by any part of the amphipathic helices and why there seems to be a differential response to cholesterol dependent on protein region. Cholesterol enrichment changes

lineshapes of the H57R1 site in a different lipid system: 80:20 POPC:POPG, the same lipid system in which cholesterol-dependent budding function was observed¹⁵⁻¹⁷ (data shown in Appendix A). This change is similar to the conformational exchange observed for the M2TMC truncation,²³ indicating that the effect of cholesterol may be membrane dependent. Possible functional changes to M2 caused by cholesterol addition to the DOPE:DOPS or DOPC:DOPS lipid systems have not been previously investigated; M2 curvature generation measured by SAXS was limited to changes in the lipid identity.¹⁸ Cholesterol has been shown to have similar intrinsic negative Gaussian curvature generation properties to those of PE lipids.⁵⁰ Cholesterol enriched membranes in this study contained a maximum of 30 mol% cholesterol, versus 80 mol% DOPE in the cubic phase proteoliposomes. This difference likely does not account for the smaller effect of cholesterol on conformational exchange in the amphipathic helices because these molecules act on the membrane and protein in different ways. For instance, the substantial cholesterol response of L43R1 combined with the demonstrated cholesterol response in the POPC:POPG lipid system suggests that cholesterol enrichment may have an effect on membrane phase dependent conformational exchange experienced by M2.

Consistent with the curvature generation properties of cholesterol, mixtures of DOPC with as little as 5 mol% cholesterol promotes formation of H_{II} phase, but cholesterol enrichment has little effect on DOPE.⁷⁴ Phase behavior of mixtures including DOPS is irregular, but 30 mol% cholesterol enrichment of DOPE:DOPS mixtures does promote H_{II} phase.⁶² It is unclear whether PE:PS mixtures experience a different phase alone than with cholesterol enrichment because there is some disagreement about the nature of phase separation induced in these mixtures.⁷⁵⁻⁷⁷ Phase information for PE:PC mixtures with

cholesterol enrichment suggest that cholesterol can induce H_{II} phase, but likely has an insignificant phase effect if H_{II} has already been induced (i.e. by PE).^{59-62,64} At approximately 25 mol% cholesterol, DOPC membranes display an irregular region of disordered phase with ambiguous curvature properties.⁷⁴ Additionally, the phase dynamics of DOPC:DOPS mixtures with cholesterol have not been characterized.

The irregularities in cholesterol's effects on the membranes used in this thesis may explain the weak effect observed in the conformational changes of the amphipathic helices. If the amphipathic helices' experience a curvature-dependent conformational change as described in Chapter 4, the absence of a change in membrane curvature when cholesterol enrichment is altered explains the observed lack of sensitivity of the L59R1 lineshape. In the DOPC:DOPS membrane, addition of cholesterol may not promote H_{II} phase and the membrane may simply retain lamellar phase, causing no change in the amphipathic helix conformation. Analogously, if the DOPE:DOPS membrane already forms H_{II} phase induced by PE, addition of cholesterol may have no effect on the membrane, causing the similar lack of an amphipathic helix conformational change. L59 is located at the end of the amphipathic helix and was not studied in the original characterization of cholesterol-dependent conformational exchange in M2TMC.²³ It is possible that the amphipathic helices do experience a cholesterol-dependent conformation, but that the change does not substantially affect the lineshape at L59R1.

The significant immobilization of the transmembrane helix labelling site, L43R1, in cholesterol enriched membranes is consistent with NMR studies suggesting that the TM domain conformation is affected by cholesterol.^{66,68,70} Drug binding to the TM region, which is dependent on channel conformation, was affected by 30 mol% cholesterol,⁶⁸ providing

further evidence that immobile, budding conformation described in this thesis shares a structurally similar TM domain with the closed channel state. Additionally, the fact that the cholesterol promoted conformation is budding-relevant¹⁵⁻¹⁷ and shares similarity with the immobile, curvature generating conformation lends further support to the hypothesis that the immobile conformation is truly the budding conformation.

5.4. Differential membrane effects to TM and AH domains explained by spontaneous curvature frustration model

Combining the results of Chapters 4 and 5 using the flexible surface model (FSM) shines light on two complications in interpreting the curvature generating conformational change in M2: First, the response to PE lipids and cholesterol appears similar, but only for the transmembrane domain labelling site, L43R1. Second, while the amphipathic helices are clearly the main driver of curvature generation, the transmembrane domain may also play a role. The differential response to cholesterol observed between the TM and AH domains of M2 may provide an explanation for the minor role that the TM domain may play in curvature generation. The flexible surface model, developed by Helfrich,⁷⁸ Gruner,⁷⁹ and Brown,⁴⁸ relates the polymorphic nature of lipid membranes to curvature induced lipid-protein interactions via the mechanism of spontaneous curvature frustration. In this model, the stress/strain of membrane curvature deformations by an integral membrane protein is relieved by balance with the chain packing energy (solvation of the transmembrane portion of the protein by the bilayer) thereby providing a source of work for protein conformational changes (Appendix D). Brown and coworkers showed that for the conformational change in rhodopsin, the free energy of the change is linearly related to the mole fraction of DOPE in the bilayer. This means that remodeling of the membrane provides the thermodynamic basis

for conformational changes that affect the shape of the protein in the bilayer. Essentially, curvature at the protein-lipid interface matches the spontaneous curvature of the membrane due to its lipid content. Enrichment of the membrane with lipid agonists such as DOPE or cholesterol or changing the bilayer thickness alters the conformational equilibrium by changing the spontaneous curvature, causing the protein to respond.^{48,80} In the case of M2, the response is tighter packing of the TM and amphipathic helices.

Interestingly, the spontaneous curvature frustration model was used to explain the irregularities of the phase transition of DOPE from H_{II} to cubic bicontinuous phase and the thermodynamic stability of the high curvature phases.⁸¹ Marsh also showed that the spontaneous curvature frustration mechanism is conceptually identical to the more commonly invoked lateral pressure profile changes at the lipid-protein interface.⁸² These two theoretical models have explained the lipid dependent conformational changes of a number of ion channel proteins, including the mechanosensitive ion channel MscL, the α -helical ion channel peptide alamethicin, and the KvAP potassium channel.⁸²⁻⁸⁴ The channel conductance of alamethicin in particular was shown to depend linearly on the mole fraction of DOPE⁸⁵ and the function of KvAP was shown to depend on cholesterol.⁸⁴

The models described in this section do not fully account for the dependence on sequence position of the effect of cholesterol on M2's conformational dynamics. Because the lateral pressure profile cannot be experimentally observed, the specific effects of cholesterol and PE lipids are unclear.^{48,86} It is possible that the substantial cholesterol effect observed at the transmembrane helix labelling site, L43R1, is due to an additional effect of cholesterol on the lateral pressure profile that is not captured by the phase alterations. Structural studies

have made extensive use of viral mimetic membranes enriched in cholesterol, finding the same immobilization of the transmembrane domain, as described above in section 5.4.^{66,70}

As discussed in Chapter 4, the amphipathic helices of M2 are unambiguously the main curvature generation region of the protein. That cholesterol stabilizes a curvature generating conformation of the amphipathic helix is also clear,⁷² and M2 has long been known as a cholesterol binding protein.¹⁴ The fact that M2 buds from cholesterol enriched 'lipid-rafts' and contains a putative cholesterol binding motif^{12,14} suggests that the function of cholesterol may not be to alter the membrane dynamics but simply to bind to and engage a conformational change in M2 directly. However, the accuracy of cholesterol binding motif prediction has long been questioned and cholesterol is known to interact with membrane proteins in a number of different ways.⁸⁷ The possible cholesterol recognition sequence in M2 does not include either L43 or L59, but occurs near the inter-helical crevice,⁸⁸ suggesting cholesterol may play a role in curvature induction that cannot be observed with the labelling sites in this chapter.

While the effect of cholesterol on the conformational dynamics of M2 cannot be elucidated with as much detail as the effect of DOPE, spontaneous curvature frustration does explain some of the relationship between the transmembrane domain and the amphipathic helices in generation of curvature. Most of the proteins whose curvature free energy dynamics have been characterized are integral proteins, like the ion channels discussed above; and while M2's ion channel functionality is modulated by lipid choice⁶⁸ and the domain may play a minor role in curvature generation,⁷³ the amphipathic helices' conformational relationship with the membrane must be characterized by the curvature frustration mechanism for the model to have validity in this system. CTP:phosphocholine

cytidyltransferase (CTC), the rate-limiting enzyme in the biosynthesis of the crucial membrane lipid, phosphatidylcholine, is activated by the binding of its amphipathic α -helix to lipid membranes. CTC has a strong activity dependence on lipid composition; in particular, DOPE enrichment to DOPC membranes promotes activity by variation of the spontaneous membrane curvature.⁸⁹ The helix binding of CTC has been shown to be well-characterized by the spontaneous curvature frustration model (Figure 5.4.1).^{32,89}

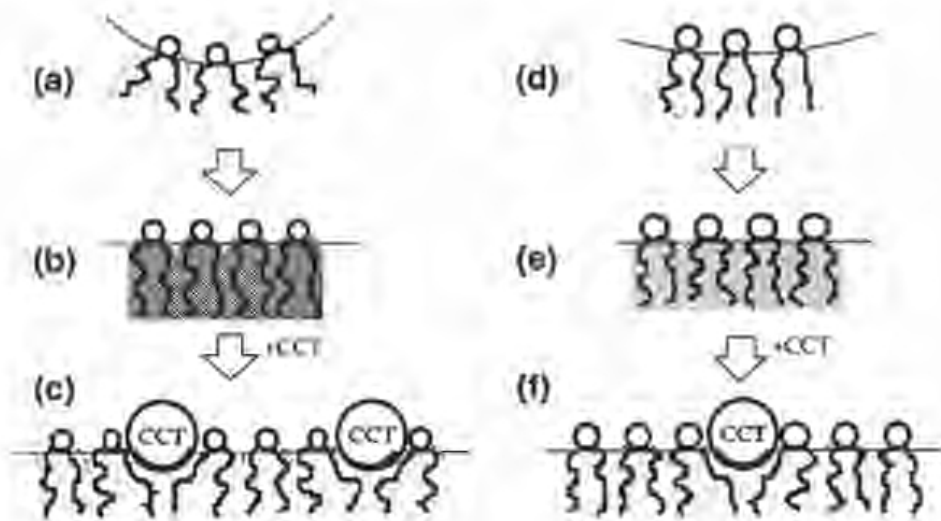


Figure 5.4.1. Illustration of spontaneous curvature frustration/relief by CTC. When a DOPE monolayer (a) is flattened (b), there is a frustration of spontaneous curvature that is relieved by binding of the CCT amphipathic helix (c). DOPC monolayers have approximately zero spontaneous curvature (d), so there is little frustration induced (e), and the free energy of binding CCT is lower, manifesting itself in fewer helices binding to the membrane and lower enzyme activation. Figure is reproduced and legend is adapted.⁸⁹

The finding that the relief of spontaneous curvature frustration can be related to amphipathic helix binding and not only transmembrane conformational changes provides further support to the hypothesis that the amphipathic helix of M2 is responsible for membrane dependent curvature generation that may secondarily affect the transmembrane domain. To answer these questions, the effect of changes to the amphipathic helix of M2 are studied in Chapter 6.

Chapter 6. Mutations in the Amphipathic Helix Alter Both Membrane Phase and Cholesterol Dependent Conformational Exchange

6.1. Introduction: Functional relevancy of the penta-Ala mutant AH construct

Membrane associated amphipathic helices are a canonical way for proteins to sense and alter membrane curvature.^{47,55,90-92} The amphipathic lipid packing sensor (ALPS) motif is the most commonly described curvature sensitive amphipathic helix unit. ALPS motifs are 20-40 amino acids sequences characterized by being repetitive and containing few charged residues. ALPS motifs are intrinsically disordered and unstructured in solution but form amphipathic helices when presented with asymmetric or intrinsically curved membranes. The ALPS motif of ArfGAP1 has been described in detail; its adsorption onto intrinsically curved membranes follows the 'Velcro model,' in which each turn of the helix senses the free energy release associated with packing onto the membrane.⁴⁷ The amphipathicity of the helix; that is the maintenance of hydrophobicity on one face, is crucial to the curvature-dependent structure and function of ALPS motifs. When two bulky, hydrophobic residues on one face of M2's amphipathic helix are mutated to alanine, budding function is abolished, showing that the hydrophobicity is responsible for curvature generation.¹⁵⁻¹⁷

6.2. CW EPR reveal curvature and cholesterol dependent conformational exchange in M2 is controlled by the amphipathicity of the C-terminal helix

To investigate the conformational effect of mutations to the amphipathic helix that affect its hydrophobicity, labelled M2 constructs were made that possess alanine mutations shown to abolish budding.¹⁷ Changes to conformational dynamics were investigated in both different membrane phase (as in Chapter 4) and in cholesterol enriched liposomes (as in Chapter 5). Figure 6.2.1 shows the CW EPR lineshapes for two selected labelling sites in the wildtype

M2 compared with the same sites in the 5Ala M2 construct, which contains these five alanine mutations. The lineshape changes observed for the transmembrane helix labelling site, L43R1, are not observed in the 5Ala construct in response to either phase or cholesterol. For both constructs, no lineshape change is observed for the amphipathic helix labelling site, H57R1, in response to phase. In Chapter 4, the other amphipathic helix sites in wildtype M2 experienced a small curvature-dependent conformational change, but these sites could not be labelled in penta-Ala because I51 and F55 are both alanine mutations. For H57, a small change is observed in response to cholesterol in penta-Ala, but not wildtype.

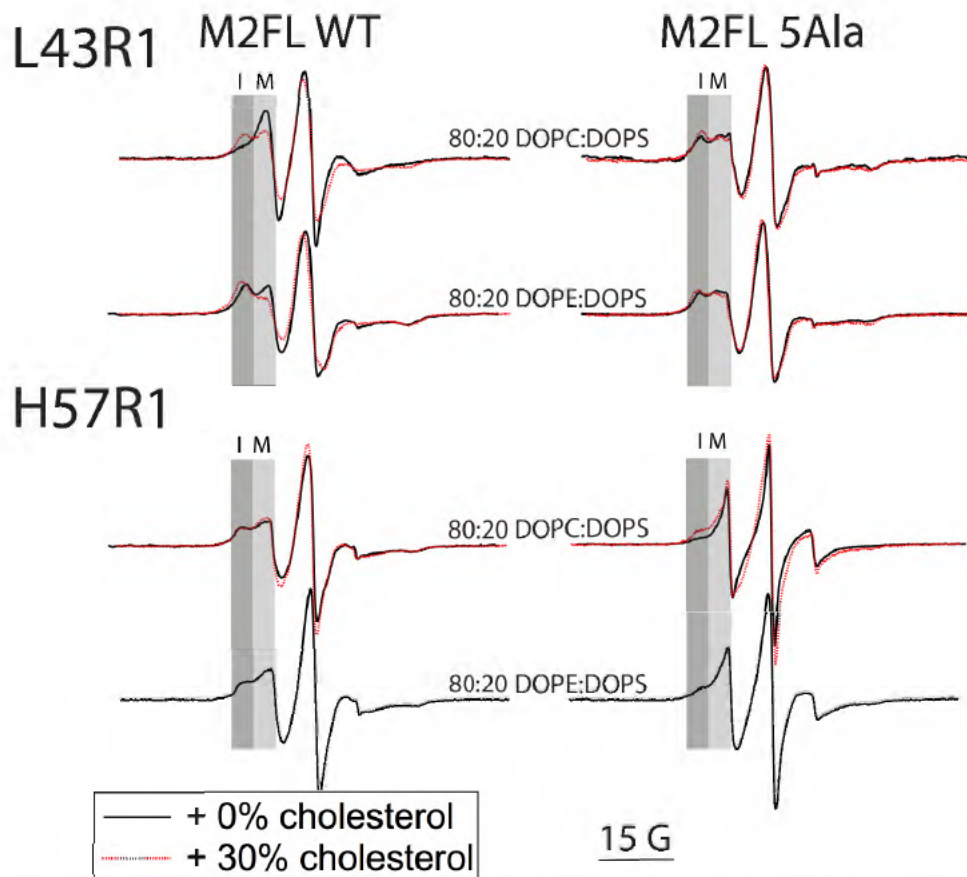


Figure 6.2.1. CW EPR lineshapes of two selected sites varying lipid environment and cholesterol enrichment for M2 wildtype (left) and penta-Ala mutant construct (right). H57R1 DOPE:DOPS with 30% cholesterol enrichment was not available at the time of writing.

Power saturation EPR experiments were conducted on both labelling sites for the

5Ala construct proteoliposomes to determine the nature of the structural changes caused by

the mutations of the amphipathic helices' hydrophobicity. Interestingly, a significant change to membrane depth is observed for L43R1, indicating that transmembrane helix in both membrane curvature environments is packed deeper in the membrane in response to these mutations. The depth of this part of the helix is similar to that observed for the wildtype M2 in cubic membrane phase, but does not appear to be curvature sensitive in 5Ala. By contrast, there is essentially no alteration to the average membrane depth of H57R1 in response to the mutations.

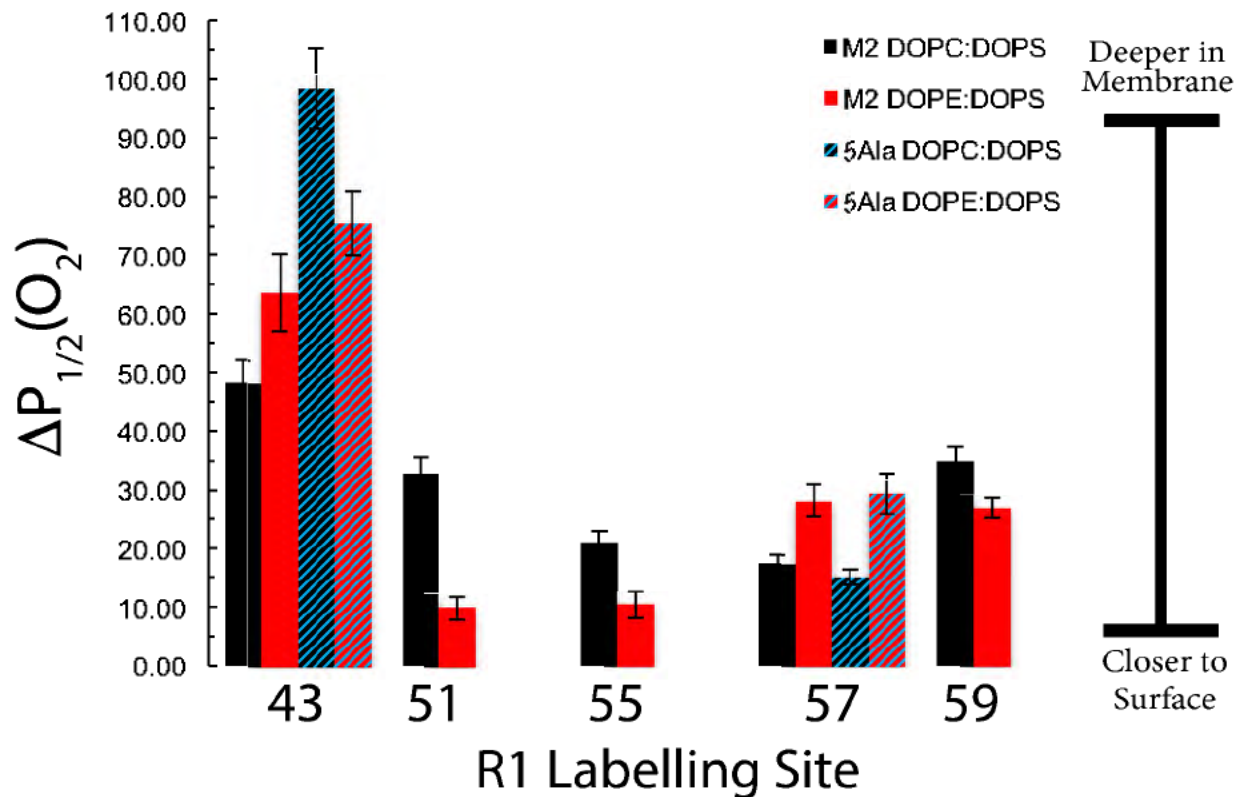


Figure 6.2.3. Oxygen power saturation for five selected labelled mutants. Lipid phase (lamellar, black and cubic, red) is varied for all sites between M2 wildtype (solid) and penta-Ala mutant constructs (cross pattern). Samples have on average four spin labels per tetramer (fully labelled). I51R1, F55R1, and L59R1 for wildtype are shown for comparison.

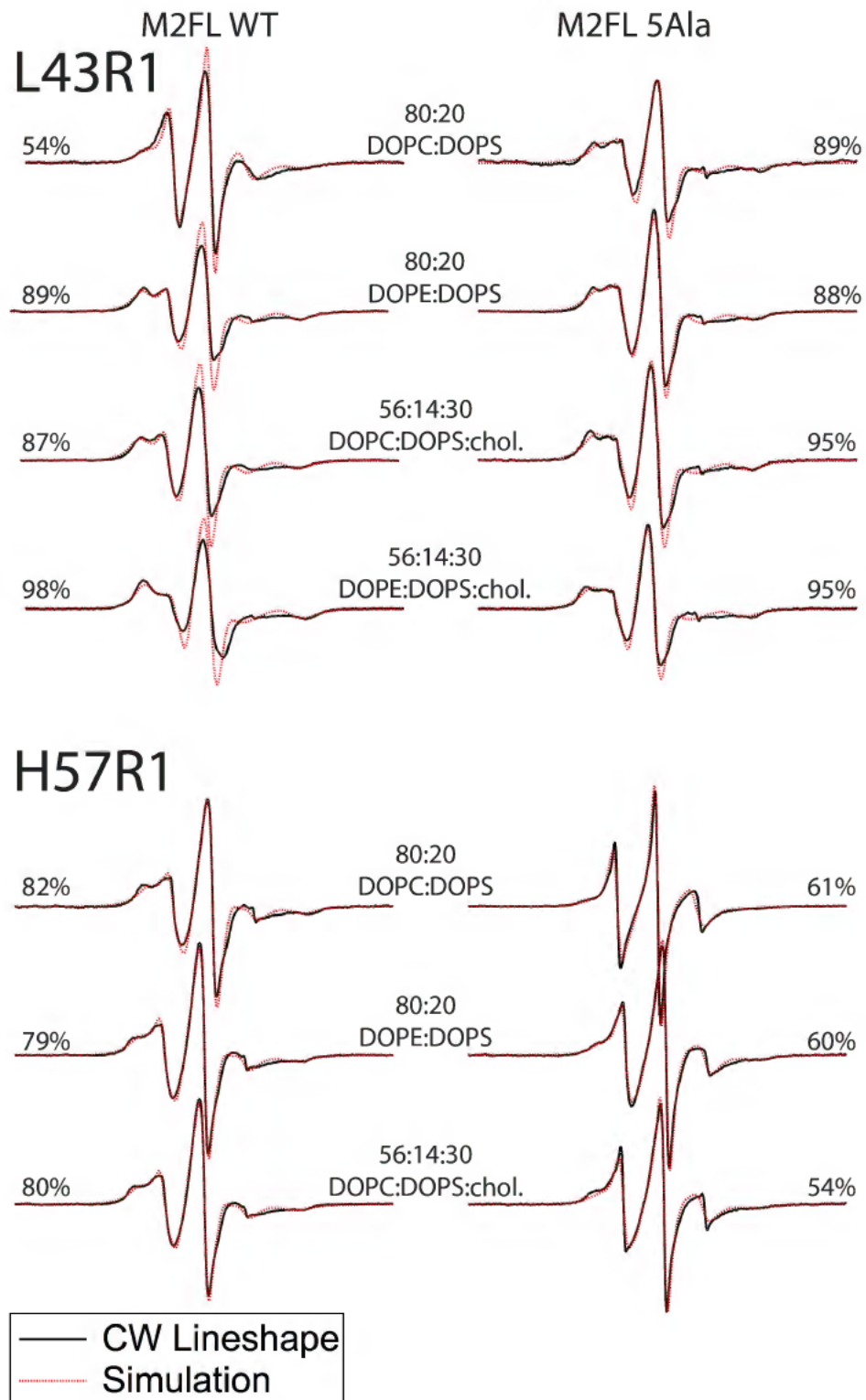


Figure 6.2.4. Spectral simulations (red) of dilute labelled CW EPR spectra (black) for two selected labelling sites for M2 wildtype (left) and penta-Ala mutant construct (right). Spectra varying membrane phase and cholesterol content are shown. Percent of immobile component population is listed to the left and right.

As in Chapters 4 and 5, simulations using the MOMD model were used to extract the population of mobile and immobile conformations represented in each of the EPR spectra. These results are shown in Figure 6.2.3. A differential effect is observed between the two labelling sites. For the 5Ala mutant, spectra of L43R1 exhibit no sensitivity to membrane curvature or presence of cholesterol. By contrast, while no shift in populations of the two conformations was observed for H57R1 in the wildtype M2, a small conformational change due to cholesterol (but not membrane curvature) is observed in the 5Ala construct. The conformational change in response to cholesterol is not an artifact of sample preparation; it was observed in several other lipid environments, confirming that H57R1 responds to cholesterol in both wildtype and 5Ala constructs (Appendix A).

6.3. Physical nature of the interaction between M2's AH and the membrane

Regardless of lipid environment, 5Ala mutations to the amphipathic helix result in an increase in mobility of H57R1. One hypothesis for this observation is that the helix becomes unstructured in the 5Ala construct, explaining the functional significance of the helical structure. Since the membrane depth of H57R1 is unchanged by the mutations, the amphipathic helix may still be associated with the membrane. However, H57 faces the solvent even when the helix is structured, suggesting that any association with the membrane that remains is weak. The observation that the amphipathic helix conformation responds to cholesterol even in the 5Ala construct is consistent with a role for cholesterol in inducing a regular structure to the helix, in an analogous manner to membrane binding.⁸⁷ This result provides an explanation for why the cholesterol response of the helix is associated with curvature induction. At the cholesterol enriched viral budzone, cholesterol may bind to M2's

amphipathic helix and stabilize its structure, allowing for a tighter membrane association that generates curvature by way of the helix's hydrophobicity.

The structural results presented here combined with the abolished budding function of the 5Ala construct strongly suggest the amphipathic helix's hydrophobicity on one face is responsible for curvature induction and that destruction of this hydrophobicity causes formation of a largely unstructured helix. Interestingly, M2's amphipathic helix has recently been shown to behave similarly to an ALPS motif, by becoming structured in association with a membrane. Circular dichroism spectroscopy confirmed the formation of a helix at the membrane surface in a lipid dependent manner; DOPE lipids promoted helix formation, suggesting a structural change in response to membrane intrinsic curvature. By contrast, when dissociated from the membrane, the amphipathic helix is unstructured.⁹³ Additionally, the membrane association was shown to promote curvature and membrane scission and this function was attributable exclusively to the hydrophobic nature of the helix. In particular, saturation transfer difference NMR indicated the presence of membrane interactions for many of the sites studied in this thesis: F47, F48, I51, Y52, F54, F55, H57, G58, and L59 were all associated with the membrane surface. These results suggest M2's amphipathic helix is a quasi-ALPS motif and was shown to be similar to the canonical ALPS protein, epsin.⁹⁴

The role of hydrophobicity of amphipathic helices in generation of curvature has been described in the context of the spontaneous curvature frustration mechanism by Kozlov and coworkers.⁹⁵ The insertion of the hydrophobic part of an amphipathic helix into a membrane was modelled using molecular dynamics. To a first approximation, hydrophobic insertion of a helix is conceptually the same as changes in transmembrane domain shape in response to curvature frustration (section 5.4). Because amphipathic helices are small, spontaneous

curvature relief varies depending on membrane depth. The curvature frustration mechanism relies on the use of free energy released by relief of frustration to drive conformational changes.^{53,79} For an amphipathic helix, conformational changes that affect the depth of the helix can change the degree of relief by altering position on an inclusion coordinate. As the amphipathic helix is inserted, spontaneous curvature increases to a maximum and then decreases as a result of the changes to lateral pressure profile (inter-lipid interactions or packing energy varies by membrane depth).^{82,86,95,96} This model provides an explanation for how the membrane depth of M2's amphipathic helix can be coupled to curvature frustration relief, thereby driving the conformational change observed in response to membrane phase. A *decrease* in membrane depth can account for a significant *increase* in curvature frustration relief by alteration of the position on the inclusion coordinate, essentially changing the curvature of the membrane by a specific change to the depth profile of the insertion.⁹⁵

This model provides an interesting explanation for how the amphipathic helices' conformational dynamics are related to changes in the transmembrane domain. Amphipathic helices have a much finer capacity for curvature relief modulation than transmembrane domains because the latter span the entire membrane depth and conformational changes as a result cannot alter the inclusion coordinate as specifically. The finding that M2's amphipathic helix is required for curvature generation, but that the transmembrane domain may be capable of reduced curvature generation can be accounted for by the difference in how these domains provide relief of curvature frustration, which can be inferred from the EPR data comparing the wildtype M2 and 5Ala constructs. One striking result of the EPR lineshape simulations is that L43R1, the transmembrane helix site, is highly immobilized in the 5Ala construct, consistent with the transmembrane domain adopting a conformation similar to the

immobile conformation in wildtype M2. By contrast, the amphipathic helix is likely unstructured, accounting for its increased mobility in the 5Ala construct. The reduced budding activity of the 5Ala mutant is therefore explained by the absence of hydrophobic insertion of the amphipathic helix. The presence of a transmembrane conformation in 5Ala presumably consistent with curvature induction provides strong evidence that the amphipathic helix is the primary driver of curvature generation, but may be assisted by a conformational change in the transmembrane domain. When the 5Ala mutations are made, the amphipathic helix becomes unstructured and hydrophobic insertion is lost, but the transmembrane domain's conformation remains immobilized. The curvature frustration model applied to wildtype and 5Ala M2 is shown in Figure 6.3.1.

Interestingly, recent work by Stachowiak and coworkers has shown that crowding of membrane proteins can promote curvature generation even when amphipathic helices have lost hydrophobicity. The role of steric bulk was found to be important in driving budding; larger proteins without amphipathic helices were found to possess curvature induction functionality if crowded enough.⁹⁷ These results may provide clues to how curvature induction by large transmembrane domains is balanced with the more specific insertion of amphipathic helices. The influence of steric bulk on curvature induction by protein crowding in particular suggests that this mechanism relies on large deformations across the insertion coordinate. Indeed, large intrinsically disordered proteins were found to generate curvature by this method.⁹⁸ In particular, the amphipathic region of epsin, the ENTH domain, is typically about 150 amino acids in length.⁹⁷ The small size of M2's amphipathic helix, combined with the demonstrated curvature induction at a variety of protein:lipid ratios¹⁸ strongly suggests M2 generates curvature not by crowding, but by hydrophobic insertion.

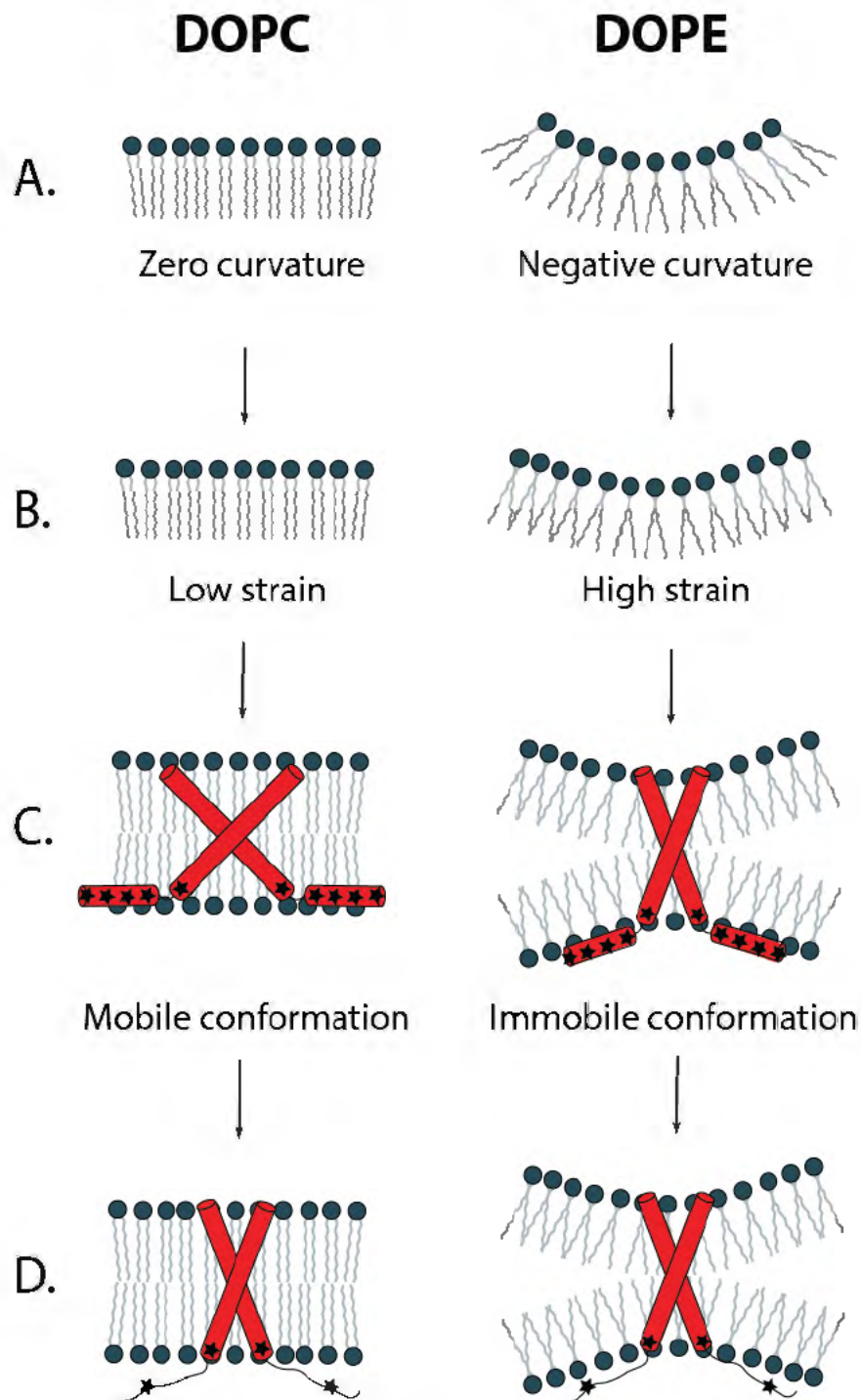


Figure 6.3.1. M2 lipid dependent curvature generation by hydrophobic insertion and spontaneous curvature frustration relief. A.) lipid spontaneous curvature, B.) curvature frustration state, C.) phase dependent relief of curvature frustration by two different conformations; the immobile conformation stabilizes the curved membrane and promotes transition to cubic phase (not shown) and subsequent scission, D.) 5Ala mutations abolish curvature inducing conformational change.

Chapter 7: Summary and Future Directions

7.1. Summary of results and model

1. *M2 has two different conformations:* M2's transmembrane domain and amphipathic helices display characteristics consistent with a two-conformation system. One conformation (mobile) features a deep amphipathic helix and loosely packed TM domain. The immobile conformation is theorized to be budding relevant because of its promotion by lipids with intrinsic curvature propensity (DOPE). It features a shallower amphipathic helix and a more tightly packed TM domain.

2. *Hydrophobic insertion is consistent with curvature induction:* Generation of curvature by the immobile conformation can be rationalized by the flexible surface model and the spontaneous curvature frustration mechanism. A balance between the stress/strain of deforming the membrane from spontaneous curvature with the packing energy of the protein into the membrane provides work for a conformational change that changes the protein's shape. The model is consistent with the amphipathic helix being the primary driver of curvature induction because it can alter the lateral pressure profile more specifically, accounting for the changes in membrane depth of the helix observed between the two conformations. The transmembrane domain may play a role in curvature induction through steric bulk or crowding.

3. *Amphipathic helix function is dependent on hydrophobicity:* As shown in previously published work, mutations that reduce the hydrophobic character of the amphipathic helices abolish budding function.^{16,17,99} The data presented in this thesis suggest this is a result of the helix becoming unstructured and losing its specific hydrophobic insertion interaction with the membrane surface. Cholesterol likely binds to the amphipathic helix regardless of mutations,

accounting for the cholesterol-dependent conformational change similar to that observed when membrane phase/curvature is changed.

7.2. Directions for future experiments

- 1. Determine role of cholesterol and membrane phase using SAXS:* While results are not available at the time of writing, we have made cysless M2 and penta-Ala samples to collect SAXS data on proteoliposomes in the lipid environments described in this thesis to characterize the specific curvature induced by different parts of M2 and the role of cholesterol. SAXS data will be collected by Nathan Schmidt at UCSF.
- 2. Investigate the degree of hydrophobicity needed for proper curvature induction:* This thesis characterized the effect of five alanine point mutations, but function is abolished by choosing any two.¹⁷ Further EPR studies of the amphipathic helix should incorporate fewer mutations with the goal of determining how hydrophobic the membrane face of the amphipathic helix must be to induce binding and curvature. Using fewer alanine mutations also frees sites on the amphipathic helix that can be used for labelling with R1.
- 3. Select EPR labelling sites suitable for DEER distances:* The conformational characterization reported here suffers from a dearth specific structural information. Double-electron-electron-resonance (DEER), a pulsed EPR experiment to measure inter-label distances, could provide information about the structure of the conformations of M2.^{21,29,41} In particular, since recent work strongly suggests the generation of curvature by spontaneous curvature frustration relief is highly shape dependent, DEER distances will be valuable for developing a more specific picture of the conformational changes to M2's shape. DEER samples have been made and will be collected by Gary Lorigan at Miami University.

Acknowledgements:

The work presented in this thesis could not have been completed without the guidance and support of my advisor, Kathleen P. Howard, who has supported our lab group's efforts at every stage. Previous Howard Group members contributed greatly to making the work presented here possible. Bryan Green '16 began the investigation of the impact of lipid intrinsic curvature on M2 conformational exchange. Megan Thompson '14 made many of the overexpressed protein growths used in the early work I did with the DOPE/DOPC/DOPS lipid system. In addition to his work characterizing cholesterol effects on M2, Shawn Kim '14 provided fitting parameters for early work using 'Multicomponent.' The Howard Lab is funded through National Institutes of Health Grant R15A1094483-01 (National Institute of Allergy and Infectious Diseases). My summer research was provided by additional support from the Mayer Davidson '57 Grant.

Our lab has benefited from collaboration with a number of talented people. DLS characterization was conducted by Dr. Catherine Crouch and Tyler Alexander '17 at Swarthmore. SR experiments were carried out by Dr. Jimmy Feix (Wisconsin Medical College in Madison.) SAXS work will be conducted by Drs. Nathan Schmidt and William DeGrado (UCSF) at the Stanford Synchrotron Radiation Lightsource.

I want to extend a great deal of thanks to my labmates Hayley Raymond '18, Grace Kim '17, and Alice Herneisen '17, all of whom contributed greatly to the joint efforts of our lab to characterize the conformations of M2. AH '17 collaborated with me extensively on the specific work presented here, in particular beginning the work with the penta-Ala construct.

Appendix A: Additional Spectra and Simulations

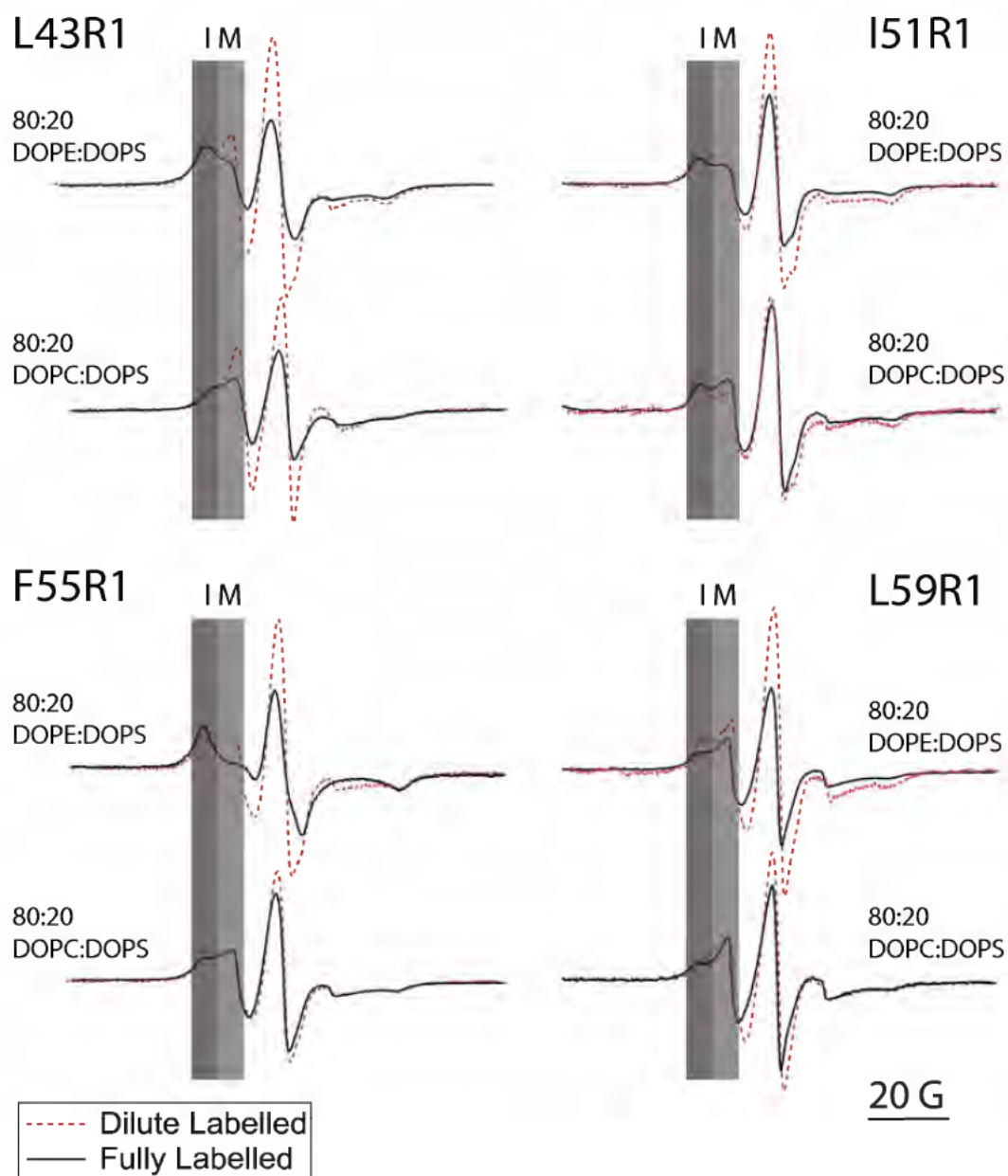


Figure A.1. Fully and dilute labelled CW EPR lineshapes for four selected sites.

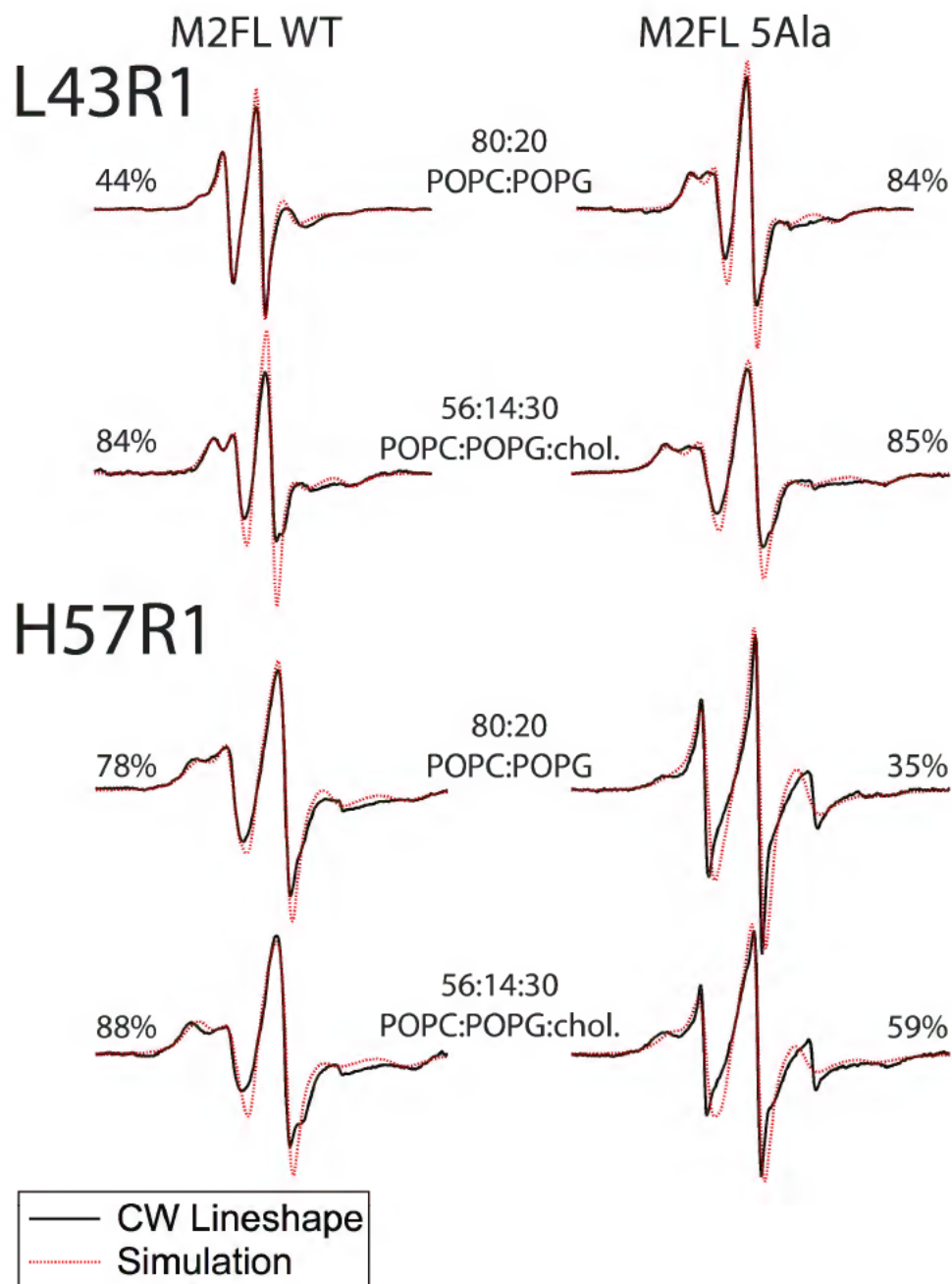


Figure A.2. Spectral simulations (red) of dilute labelled CW EPR spectra (black) for two selected labelling sites for M2 wildtype (left) and penta-Ala mutant construct (right). Lamellar phase POPC:POPG lipid environment with and without 30% cholesterol are shown. Percent of immobile component population is listed to the left and right.

Appendix B: MOMD model simulation parameters

Protein	Lipid mix	% mobile	% immobile	t, mobile (ns)	t, immobile (ns)	Mobile			Immobile			Mobile			Immobile			g _{zx}	g _{yy}	g _{zz}
						A _{xx}	A _{yy}	A _{zz}	A _{zz}	A _{yy}	A _{zz}	R _{xx}	R _{yy}	R _{zz}	R _{xx}	R _{yy}	R _{zz}			
43	PE	11	89	2.12	7.07	4.3	5.2	35.25	5	4.79	37.37	7.56	8.2	7.93	7.52	7.4	7.2	2.00845	2.00566	2.00188
43	PE chol	2	98	2.12	7.07	4.3	5.2	35.25	5	4.79	37.37	7.56	8.2	7.93	7.52	7.4	7.2	2.00845	2.00566	2.00188
43	PC	46	54	2.12	7.07	4.3	5.2	35.25	5	4.79	37.37	7.56	8.2	7.93	7.52	7.4	7.2	2.00845	2.00566	2.00188
43	PC chol	13	87	2.12	7.07	4.3	5.2	35.25	5	4.79	37.37	7.56	8.2	7.93	7.52	7.4	7.2	2.00845	2.00566	2.00188
43 5Ala	PE	12	88	3.46	8.06	4.3	5.2	35.25	5	4.79	37.37	6.91	8.35	7.79	7.63	7.38	6.94	2.00845	2.00566	2.00188
43 5Ala	PE chol	5	95	3.46	8.06	4.3	5.2	35.25	5	4.79	37.37	6.91	8.35	7.79	7.63	7.38	6.94	2.00845	2.00566	2.00188
43 5Ala	PC	11	89	3.46	8.06	4.3	5.2	35.25	5	4.79	37.37	6.91	8.35	7.79	7.63	7.38	6.94	2.00845	2.00566	2.00188
43 5Ala	PC chol	5	95	3.46	8.06	4.3	5.2	35.25	5	4.79	37.37	6.91	8.35	7.79	7.63	7.38	6.94	2.00845	2.00566	2.00188
51	PE	16	84	3.56	9.9	4.7	4.5	37.23	5.1	4.69	37.38	7.6	7.46	7.94	7.33	6.73	7.62	2.00845	2.00566	2.00188
51	PC	22	78	3.56	9.9	4.7	4.5	37.23	5.1	4.69	37.38	7.6	7.46	7.94	7.33	6.73	7.62	2.00845	2.00566	2.00188
55	PE	22	78	3.56	8.49	4.7	4.5	37.23	5.1	4.69	37.38	7.6	7.46	7.94	7.93	6.23	7.72	2.00845	2.00566	2.00188
55	PC	34	66	3.56	8.49	4.7	4.5	37.23	5.1	4.69	37.38	7.6	7.46	7.94	7.93	6.23	7.72	2.00845	2.00566	2.00188
57	PE	21	79	3.1	9.64	4.7	4.5	37.23	5.1	4.69	37.38	7.29	8.09	7.82	6.97	7.02	7.72	2.00845	2.00566	2.00188
57	PC	18	82	3.1	9.64	4.7	4.5	37.23	5.1	4.69	37.38	7.29	8.09	7.82	6.97	7.02	7.72	2.00845	2.00566	2.00188
57	PC chol	20	80	3.1	9.64	4.7	4.5	37.23	5.1	4.69	37.38	7.29	8.09	7.82	6.97	7.02	7.72	2.00845	2.00566	2.00188
57 5Ala	PE	60	40	3.1	9.64	4.7	4.5	37.23	5.1	4.69	37.38	7.29	8.09	7.82	6.97	7.02	7.72	2.00845	2.00566	2.00188
57 5Ala	PC	61	39	3.1	9.64	4.7	4.5	37.23	5.1	4.69	37.38	7.29	8.09	7.82	6.97	7.02	7.72	2.00845	2.00566	2.00188
57 5Ala	chol	54	46	3.1	9.64	4.7	4.5	37.23	5.1	4.69	37.38	7.29	8.09	7.82	6.97	7.02	7.72	2.00845	2.00566	2.00188
59	PE	31	69	4.93	9.79	4.7	4.5	37.23	5.1	4.69	37.38	6.82	8	7.76	7.25	6.69	7.76	2.00845	2.00566	2.00188
59	PE chol	35	65	4.93	9.79	4.7	4.5	37.23	5.1	4.69	37.38	6.82	8	7.76	7.25	6.69	7.76	2.00845	2.00566	2.00188
59	PC	40	60	4.93	9.79	4.7	4.5	37.23	5.1	4.69	37.38	6.82	8	7.76	7.25	6.69	7.76	2.00845	2.00566	2.00188
59	PC chol	35	65	4.93	9.79	4.7	4.5	37.23	5.1	4.69	37.38	6.82	8	7.76	7.25	6.69	7.76	2.00845	2.00566	2.00188
43	PCPG	56	44	2.47	8.78	4.3	5.2	35.25	5	4.79	37.37	6.67	8.16	8.66	7.68	6.93	7.22	2.00845	2.00566	2.00188
43	PCPG chol	16	84	2.47	8.78	4.3	5.2	35.25	5	4.79	37.37	6.67	8.16	8.66	7.68	6.93	7.22	2.00845	2.00566	2.00188
43 5Ala	PCPG	16	84	2.47	8.78	4.3	5.2	35.25	5	4.79	37.37	6.67	8.16	8.66	7.68	6.93	7.22	2.00845	2.00566	2.00188
43 5Ala	PCPG chol	15	85	2.47	8.78	4.3	5.2	35.25	5	4.79	37.37	6.67	8.16	8.66	7.68	6.93	7.22	2.00845	2.00566	2.00188
57	PCPG	22	78	3.1	10.4	4.7	4.5	37.23	5.1	4.69	37.38	7.29	8.09	7.82	6.97	6.92	7.72	2.00845	2.00566	2.00188
57	PCPG chol	12	88	3.1	10.4	4.7	4.5	37.23	5.1	4.69	37.38	7.29	8.09	7.82	6.97	6.92	7.72	2.00845	2.00566	2.00188
57 5Ala	PCPG	65	35	3.1	10.4	4.7	4.5	37.23	5.1	4.69	37.38	7.29	8.09	7.82	6.97	6.92	7.72	2.00845	2.00566	2.00188
57 5Ala	PCPG chol	41	59	3.1	10.4	4.7	4.5	37.23	5.1	4.69	37.38	7.29	8.09	7.82	6.97	6.92	7.72	2.00845	2.00566	2.00188

Appendix C: Experimental Data Tables

Power saturation data

Protein	Lipid	Power saturation					
		Oxygen $P_{1/2}$	Oxygen error	Nitrogen $P_{1/2}$	Nitrogen Error	$\Delta P_{1/2}$	Δ error
43	PE	87.57	6.18	23.86	2.17	63.71	6.55
43	PE chol	29.81	1.27	16.53	0.91	13.28	1.56
43	PC	71.76	2.13	23.61	3.32	48.15	3.94
43	PC chol	51.25	3.11	21.07	1.74	30.18	3.56
51	PE	22.52	1.68	12.54	0.84	9.98	1.88
51	PC	49.34	2.21	16.57	1.80	32.77	2.85
55	PE	20.75	1.90	10.23	0.99	10.51	2.14
55	PC	41.04	1.33	20.03	1.33	21.00	1.88
57	PE	19.44	1.53	47.62	2.26	28.18	2.72
57	PC	18.89	1.40	36.26	0.66	17.36	1.54
59	PE	45.09	1.52	18.14	0.85	26.95	1.74
59	PC	51.88	2.17	16.99	0.98	34.89	2.38

CW Spectral Data

Site	Lipid	Ddute											
		left (g)	error	right (g)	error	max	error	min	error	ΔH (G)	ΔH error (G)	ΔH^1 (G ²)	ΔH^1 error (G ²)
43	PE	3480.80	0.29	3485.80	0.00	3481.10	2.10	1333.50	0.00	5.00	0.29	0.20	0.01
43	PE chol	3475.50	0.14	3483.60	0.10	1036.70	3.50	-718.30	1.50	8.10	0.17	0.12	0.00
43	PC	3476.60	0.00	3480.70	0.00	1363.00	0.00	1338.50	0.00	4.10	0.00	0.24	0.00
43	PC chol	3475.80	0.29	3481.00	0.14	1042.80	4.00	-805.60	3.60	5.20	0.32	0.19	0.01
51	PE	3475.20	0.43	3480.40	0.00	1833.50	8.00	1201.50	0.00	5.20	0.43	0.19	0.02
51	PC	3475.20	0.29	3480.10	0.43	1370.70	0.75	1071.40	18.90	4.90	0.52	0.20	0.02
55	PE	3476.60	0.43	3481.70	0.58	1820.70	6.30	1235.70	22.50	5.10	0.72	0.20	0.03
55	PC	3478.20	0.29	3482.60	0.29	1324.80	5.40	-963.60	4.20	4.40	0.41	0.23	0.02
57	PE	3478.30	0.29	3481.80	0.14	1442.30	2.45	1278.20	0.00	3.50	0.32	0.29	0.03
57	PC	3481.80	0.29	3485.20	0.14	1165.60	2.80	-976.00	0.00	3.40	0.32	0.29	0.03
59	PE	3476.60	0.00	3480.20	0.14	1962.90	0.00	1476.90	0.00	3.60	0.14	0.28	0.01
59	PE chol	3478.80	0.10	3482.10	0.14	1012.60	1.60	-943.50	11.00	3.30	0.17	0.30	0.02
59	PC	3477.90	0.14	3480.80	0.14	1532.50	1.00	1310.00	5.50	2.90	0.20	0.34	0.02
59	PC chol	3477.60	0.29	3481.00	0.14	1014.20	8.75	1005.00	0.00	3.40	0.32	0.29	0.03

Site	Lipid	Fully											Ω	Ω error	
		left (g)	error	right (g)	error	max	error	min	error	ΔH (G)	ΔH error (G)	ΔH^1 (G ²)			ΔH^1 error (G ²)
43	PE	3478.20	0.00	3486.70	0.00	778.40	0.00	-646.10	0.00	8.50	0.00	0.12	0.00	0.00	0.25

43	PE chol	3477.30	0.14	3485.80	0.58	501.50	2.00	-424.00	4.50	8.50	0.60	0.12	0.01	0.01	0.16
43	PC	3477.00	0.14	3482.30	0.29	718.50	1.50	-580.50		5.30	0.32	0.19	0.01	0.00	0.27
43	PC chol	3475.80	0.43	3484.20	0.73	400.00	1.60	-325.60	2.80	8.40	0.85	0.12	0.01	0.01	0.23
51	PE	3476.80	0.29	3482.10	0.27	1079.50	2.50	-726.50	1.00	5.30	0.40	0.19	0.01	0.00	0.25
51	PC	3477.60	0.00	3482.30	0.14	1272.00	0.00	-959.50	0.00	4.70	0.14	0.21	0.01	0.00	0.25
55	PE	3475.50	0.29	3485.40	0.73	964.00	5.40	-768.60	3.60	9.90	0.79	0.10	0.01	0.00	0.13
55	PC	3476.00	0.29	3480.50	0.00	1048.80	5.40	-832.20	0.00	4.50	0.29	0.22	0.01	0.00	0.13
57	PC														
57	PE														
59	PE	3477.40	0.00	3481.00	0.14	994.05	0.00	-891.45	3.00	3.60	0.14	0.28	0.01	0.00	0.21
59	PE chol	3477.40	0.14	3481.10	0.14	549.25	2.00	-455.75	4.75	3.70	0.20	0.27	0.01	0.01	0.16
59	PC	3477.70	0.14	3480.80	0.12	1153.00	3.00	1068.50	0.00	3.10	0.18	0.32	0.02	0.00	0.21
59	PC chol	3479.20	0.14	3481.70	0.14	1103.80	7.00	1085.00	8.50	2.50	0.20	0.40	0.03	0.00	0.08

Appendix D: Spontaneous Curvature Frustration Model

Brown and coworkers developed the spontaneous curvature frustration mechanism to explain the conformational change in rhodopsin, an integral G-protein coupled receptor. The key quantity is the curvature free energy, g_c , the work needed to deform the bilayer from its spontaneous curvature, H_0 , to its actual curvature, H_i . In this case, both H_i and H_0 are defined as mean curvatures, the average of the opposite leaflet principal curvatures, c_1 and c_2 (section 4.1). Then, the curvature free energy is defined as

$$g_c = \kappa(H_i^L - H_0^L)^2 + \bar{\kappa}K.$$

The quantities, κ and $\bar{\kappa}$, are the bending rigidity and the modulus of Gaussian curvature, respectively. The curvature free energy is balanced with the chain packing energy, γA_i^P , where γ is the 'interfacial tension,' the work needed for lipids to solvate the transmembrane part of the protein, and A_i^P is the area of the protein contacting the bilayer. The balance of the chain packing energy and the curvature free energy leads to the following equation for the free energy change associated with the transition between two conformations, I and II,

$$G_o = \kappa(H_{II}^L - H_0^L)^2 - \kappa(H_I^L - H_0^L)^2 + \gamma(A_{II}^P - A_I^P).$$

State II is known to have a larger surface area, so the last term is positive. Then, if the bilayer curvature changes, the curvature stress balances and this is coupled to the work needed for the protein to change conformations.⁸⁰ This analysis has been developed in much more detail and complexity in the other work of Brown⁴⁸ and Marsh,^{82,83} and most notably, has been applied to the hydrophobic insertion of amphipathic helices.^{53,83,95}

References:

1. Nicholson KG, Wood JM, Zambon M. Influenza. *Lancet*. 2003;362(9397):1733-1745. doi:[http://dx.doi.org/10.1016/S0140-6736\(03\)14854-4](http://dx.doi.org/10.1016/S0140-6736(03)14854-4).
2. Krug RM, Aramini JM. Emerging antiviral targets for influenza A virus. *Trends Pharmacol Sci*. 2009;30(6):269-277. doi:10.1016/j.tips.2009.03.002.
3. Fiorin G, Carnevale V, DeGrado WF. The Flu's Proton Escort. *Science (80-)*. 2010;330(6003):456-458. <http://science.sciencemag.org/content/330/6003/456.abstract>.
4. Schnell JR, Chou JJ. Structure and mechanism of the M2 proton channel of influenza A virus. *Nature*. 2008;451(7178):591-595. doi:10.1038/nature06531.
5. Du J, Cross TA, Zhou H-X. Recent progress in structure-based anti-influenza drug design. *Drug Discov Today*. 2012;17(19-20):1111-1120. doi:10.1016/j.drudis.2012.06.002.
6. Lamb RA, Zebedee SL, Richardson CD. Influenza virus M2 protein is an integral membrane protein expressed on the infected-cell surface. *Cell*. 1985;40(3):627-633. doi:10.1016/0092-8674(85)90211-9.
7. Pinto LH, Holsinger LJ, Lamb RA. Influenza virus M2 protein has ion channel activity. *Cell*. 1992;69(3):517-528. <http://www.ncbi.nlm.nih.gov/pubmed/1374685>. Accessed April 5, 2017.
8. Tian C, Gao PF, Pinto LH, Lamb RA, Cross TA. Initial structural and dynamic characterization of the M2 protein transmembrane and amphipathic helices in lipid bilayers. *Protein Sci*. 2009;12(11):2597-2605. doi:10.1110/ps.03168503.
9. McCown MF, Pekosz A. The Influenza A Virus M2 Cytoplasmic Tail Is Required for Infectious Virus Production and Efficient Genome Packaging. *J Virol*. 2005;79(6):3595-3605. doi:10.1128/JVI.79.6.3595-3605.2005.
10. Stewart SM, Pekosz A. Mutations in the Membrane-Proximal Region of the Influenza A Virus M2 Protein Cytoplasmic Tail Have Modest Effects on Virus Replication. *J Virol*. 2011;85(23):12179-12187. doi:10.1128/JVI.05970-11.
11. Iwatsuki-Horimoto K, Horimoto T, Noda T, et al. The Cytoplasmic Tail of the Influenza A Virus M2 Protein Plays a Role in Viral Assembly. *J Virol*. 2006;80(11):5233-5240. doi:10.1128/JVI.00049-06.
12. Veit M, Thaa B. Association of influenza virus proteins with membrane rafts. *Adv Virol*. 2011;2011:370606. doi:10.1155/2011/370606.
13. Zhang J, Pekosz A, Lamb RA. Influenza virus assembly and lipid raft microdomains: a role for the cytoplasmic tails of the spike glycoproteins. *J Virol*. 2000;74(10):4634-4644. <http://www.ncbi.nlm.nih.gov/pubmed/10775599>. Accessed April 5, 2017.
14. Schroeder C, Heider H, Moncke-Buchner E, Lin T-I. The influenza virus ion channel and maturation cofactor M2 is a cholesterol-binding protein. *Eur Biophys J*. 2005;34(1):52-66. doi:10.1007/s00249-004-0424-1.
15. Rossman JS, Jing X, Leser GP, Balannik V, Pinto LH, Lamb RA. Influenza virus M2 ion channel protein is necessary for filamentous virion formation. *J Virol*. 2010;84(10):5078-5088. doi:10.1128/JVI.00119-10.
16. Rossman JS, Jing X, Leser GP, Lamb RA. Influenza Virus M2 Protein Mediates ESCRT-Independent Membrane Scission. *Cell*. 2010;142(6):902-913. doi:10.1016/j.cell.2010.08.029.

17. Roberts KL, Leser GP, Ma C, Lamb RA. The amphipathic helix of influenza A virus M2 protein is required for filamentous bud formation and scission of filamentous and spherical particles. *J Virol.* 2013;87(18):9973-9982. doi:10.1128/JVI.01363-13.
18. Schmidt NW, Mishra A, Wang J, DeGrado WF, Wong GCL. Influenza Virus A M2 Protein Generates Negative Gaussian Membrane Curvature Necessary for Budding and Scission. *J Am Chem Soc.* 2013;135(37):13710-13719. doi:10.1021/ja400146z.
19. Klug CS, Feix JB. Methods and Applications of Site-Directed Spin Labeling EPR Spectroscopy. In: *Methods in Cell Biology.* Vol 84. ; 2008:617-658. doi:10.1016/S0091-679X(07)84020-9.
20. Altenbach C, López CJ, Hideg K, Hubbell WL. Exploring Structure, Dynamics, and Topology of Nitroxide Spin-Labeled Proteins Using Continuous-Wave Electron Paramagnetic Resonance Spectroscopy. In: *Methods in Enzymology.* Vol 564. ; 2015:59-100. doi:10.1016/bs.mie.2015.08.006.
21. Sahu ID, Lorigan GA. Biophysical EPR Studies Applied to Membrane Proteins. *J Phys Chem Biophys.* 2015;5(6). doi:10.4172/2161-0398.1000188.
22. Huang S, Green B, Thompson M, et al. C-terminal juxtamembrane region of full-length M2 protein forms a membrane surface associated amphipathic helix. *Protein Sci.* 2015;24(3):426-429. doi:10.1002/pro.2631.
23. Kim SS, Upshur MA, Saotome K, et al. Cholesterol-Dependent Conformational Exchange of the C-Terminal Domain of the Influenza A M2 Protein. *Biochemistry.* 2015;54(49):7157-7167. doi:10.1021/acs.biochem.5b01065.
24. Saotome K, Duong-Ly KC, Howard KP. Influenza A M2 protein conformation depends on choice of model membrane. *Pept Sci.* 2015;104(4):405-411. doi:10.1002/bip.22617.
25. Nguyen PA, Soto CS, Polishchuk A, et al. pH-induced conformational change of the influenza M2 protein C-terminal domain. *Biochemistry.* 2008;47(38):9934-9936. doi:10.1021/bi801315m.
26. Duong-Ly KC, Nanda V, DeGrado WF, Howard KP. The conformation of the pore region of the M2 proton channel depends on lipid bilayer environment. *Protein Sci.* 2005;14(4):856-861. doi:10.1110/ps.041185805.
27. Weil JA, Bolton JR, Wertz JE. Electron Paramagnetic Resonance: Elementary Theory and Practical Applications. *J Magn Reson Ser A.* 1994;113:664. doi:10.1006/jmra.1995.1071.
28. Columbus L. Electron Paramagnetic Resonance.
29. Sahu ID, McCarrick RM, Lorigan GA. Use of electron paramagnetic resonance to solve biochemical problems. *Biochemistry.* 2013;52(35):5967-5984. doi:10.1021/bi400834a.
30. Kroncke BM, Horanyi PS, Columbus L. Structural origins of nitroxide side chain dynamics on membrane protein α -helical sites. *Biochemistry.* 2010;49(47):10045-10060. doi:10.1021/bi101148w.
31. Columbus L, Kálai T, Jekő J, Hideg K, Hubbell W. Molecular Motion of Spin Labeled Side Chains in α -Helices: Analysis by Variation of Side Chain Structure. *Biochemistry.* 2001;40(13):3828-3846. doi:10.1021/BI002645H.
32. Fleissner MR, Cascio D, Hubbell WL. Structural origin of weakly ordered nitroxide motion in spin-labeled proteins. *Protein Sci.* 2009;18(5):893-908. doi:10.1002/pro.96.
33. Budil DE, Lee S, Saxena S, Freed JH. Nonlinear-Least-Squares Analysis of Slow-

- Motion EPR Spectra in One and Two Dimensions Using a Modified Levenberg–Marquardt Algorithm. *J Magn Reson Ser A*. 1996;120(2):155-189. doi:10.1006/jmra.1996.0113.
34. Columbus L, Hubbell WL. Mapping backbone dynamics in solution with site-directed spin labeling: GCN4-58 bZip free and bound to DNA. *Biochemistry*. 2004;43(23):7273-7287. doi:10.1021/bi0497906.
 35. Bridges MD, Hideg K, Hubbell WL. Resolving Conformational and Rotameric Exchange in Spin-Labeled Proteins Using Saturation Recovery EPR. *Appl Magn Reson*. 2010;37(1-4):363-390. doi:10.1007/s00723-009-0079-2.
 36. Columbus L, Hubbell WL. A new spin on protein dynamics. *Trends Biochem Sci*. 2002;27(6):288-295. doi:10.1016/S0968-0004(02)02095-9.
 37. Yang Z, Bridges M, Lerch MT, Altenbach C, Hubbell WL. Chapter One – Saturation Recovery EPR and Nitroxide Spin Labeling for Exploring Structure and Dynamics in Proteins. In: *Methods in Enzymology*. Vol 564. ; 2015:3-27. doi:10.1016/bs.mie.2015.07.016.
 38. Guo Z, Cascio D, Hideg K, Hubbell WL. Structural determinants of nitroxide motion in spin-labeled proteins: Solvent-exposed sites in helix B of T4 lysozyme. *Protein Sci*. 2008;17(2):228-239. doi:10.1110/ps.073174008.
 39. Guo Z, Cascio D, Hideg K, Kálai T, Hubbell WL. Structural determinants of nitroxide motion in spin-labeled proteins: Tertiary contact and solvent-inaccessible sites in helix G of T4 lysozyme. *Protein Sci*. 2007;16(6):1069-1086. doi:10.1110/ps.062739107.
 40. López CJ, Fleissner MR, Guo Z, Kusnetzow AK, Hubbell WL. Osmolyte perturbation reveals conformational equilibria in spin-labeled proteins. *Protein Sci*. 2009;18(8):1637-1652. doi:10.1002/pro.180.
 41. Sahu ID, McCarrick RM, Troxel KR, et al. DEER EPR Measurements for Membrane Protein Structures via Bifunctional Spin Labels and Lipodisq Nanoparticles. *Biochemistry*. 2013;52(38):6627-6632. doi:10.1021/bi4009984.
 42. Earle KA, Budil DE. Calculating Slow-Motion ESR Spectra of Spin-Labeled Polymers. In: *Advanced ESR Methods in Polymer Research*. Hoboken, NJ, USA: John Wiley & Sons, Inc.; 2006:53-83. doi:10.1002/047005350X.ch3.
 43. Chiang Y-W, Zheng T-Y, Kao C-J, Horng J-C. Determination of Interspin Distance Distributions by cw-ESR Is a Single Linear Inverse Problem. *Biophys J*. 2009;97(3):930-936. doi:10.1016/j.bpj.2009.05.030.
 44. Christian Altenbach ‡, Kyoung-Joon Oh ‡ §, René J. Trabanino ‡, Kálmán Hideg I and, Wayne L. Hubbell* ‡. Estimation of Inter-Residue Distances in Spin Labeled Proteins at Physiological Temperatures: Experimental Strategies and Practical Limitations†. *Biochemistry*. 2001;40(51):15471-15482. doi:10.1021/BI011544W.
 45. Rand RP, Fuller NL, Gruner SM, Parsegian VA. Membrane curvature, lipid segregation, and structural transitions for phospholipids under dual-solvent stress. *Biochemistry*. 1990;29(1):76-87. doi:10.1021/bi00453a010.
 46. Marsh D. Polarity and permeation profiles in lipid membranes. *Proc Natl Acad Sci U S A*. 2001;98(14):7777-7782. doi:10.1073/pnas.131023798.
 47. Zimmerberg J, Kozlov MM. How proteins produce cellular membrane curvature. *Nat Rev Mol Cell Biol*. 2006;7(1):9-19. doi:10.1038/nrm1784.
 48. Brown MF. Curvature forces in membrane lipid-protein interactions. *Biochemistry*. 2012;51(49):9782-9795. doi:10.1021/bi301332v.

49. Siegel DP, Kozlov MM. The Gaussian Curvature Elastic Modulus of N-Monomethylated Dioleoylphosphatidylethanolamine: Relevance to Membrane Fusion and Lipid Phase Behavior. *Biophys J*. 2004;87(1):366-374. doi:10.1529/biophysj.104.040782.
50. Kollmitzer B, Heftberger P, Rappolt M, Pabst G. Monolayer spontaneous curvature of raft-forming membrane lipids. *Soft Matter*. 2013;9(45):10877-10884. doi:10.1039/C3SM51829A.
51. Shearman GC, Ces O, Templer RH, Seddon JM. Inverse lyotropic phases of lipids and membrane curvature. *J Phys Condens Matter*. 2006;18(28):S1105-S1124. doi:10.1088/0953-8984/18/28/S01.
52. Schmidt NW, Lis M, Zhao K, et al. Molecular basis for nanoscopic membrane curvature generation from quantum mechanical models and synthetic transporter sequences. *J Am Chem Soc*. 2012;134(46):19207-19216. doi:10.1021/ja308459j.
53. Baumgart T, Capraro BR, Zhu C, Das SL. Thermodynamics and Mechanics of Membrane Curvature Generation and Sensing by Proteins and Lipids. *Annu Rev Phys Chem*. 2011;62(1):483-506. doi:10.1146/annurev.physchem.012809.103450.
54. Phillips R, Ursell T, Wiggins P, Sens P. Emerging roles for lipids in shaping membrane-protein function. *Nature*. 2009;459(7245):379-385. doi:10.1038/nature08147.
55. McMahon HT, Gallop JL. Membrane curvature and mechanisms of dynamic cell membrane remodelling. *Nature*. 2005;438(7068):590-596. doi:10.1038/nature04396.
56. Opekarov M, Tanner W. Specific lipid requirements of membrane proteins - A putative bottleneck in heterologous expression. *Biochim Biophys Acta - Biomembr*. 2003;1610(1):11-22. doi:10.1016/S0005-2736(02)00708-3.
57. Bogdanov M, Heacock PN, Dowhan W. A polytopic membrane protein displays a reversible topology dependent on membrane lipid composition. *EMBO J*. 2002;21(9):2107-2116. doi:10.1093/emboj/21.9.2107.
58. Vitrac H, Bogdanov M, Dowhan W. In vitro reconstitution of lipid-dependent dual topology and postassembly topological switching of a membrane protein. *Proc Natl Acad Sci*. 2013;110(23):9338-9343. doi:10.1073/pnas.1304375110.
59. Tilcock CPS. Lipid polymorphism. *Chem Phys Lipids*. 1986;40(2-4):109-125. doi:10.1016/0009-3084(86)90066-6.
60. Tilcock CPS, Cullis PR. Lipid Polymorphism. *Ann N Y Acad Sci*. 1987;492(1):88-102. doi:10.1111/J.1749-6632.1987.TB48657.X.
61. Tilcock CP, Bally MB, Farren SB, Cullis PR. Influence of cholesterol on the structural preferences of dioleoylphosphatidylethanolamine-dioleoylphosphatidylcholine systems: a phosphorus-31 and deuterium nuclear magnetic resonance study. *Biochemistry*. 1982;21(19):4596-4601. doi:10.1021/bi00262a013.
62. Bally MB, Tilcock CP, Hope MJ, Cullis PR. Polymorphism of phosphatidylethanolamine-phosphatidylserine model systems: influence of cholesterol and Mg²⁺ on Ca²⁺-triggered bilayer to hexagonal (HII) transitions. *Can J Biochem cell Biol*. 1983;61(6):346-352. <http://www.ncbi.nlm.nih.gov/pubmed/6883167>. Accessed April 6, 2017.
63. Tilcock CPS, Cullis PR. The polymorphic phase behavior of mixed phosphatidylserine-phosphatidylethanolamine model systems as detected by ³¹P-NMR. Effects of divalent cations and pH. *BBA - Biomembr*. 1981;641(1):189-201.

- doi:10.1016/0005-2736(81)90583-6.
64. Tilcock CP, Bally MB, Farren SB, Cullis PR, Gruner SM. Cation-dependent segregation phenomena and phase behavior in model membrane systems containing phosphatidylserine: influence of cholesterol and acyl chain composition. *Biochemistry*. 1984;23(12):2696-2703. <http://www.ncbi.nlm.nih.gov/pubmed/6466608>. Accessed April 6, 2017.
 65. Hope MJ, Cullis PR. The bilayer stability of inner monolayer lipids from the human erythrocyte. *FEBS Lett*. 1979;107(2):323-326. doi:10.1016/0014-5793(79)80399-3.
 66. Hu F, Luo W, Cady SD, Hong M. Conformational plasticity of the influenza A M2 transmembrane helix in lipid bilayers under varying pH, drug binding, and membrane thickness. *Biochim Biophys Acta - Biomembr*. 2011;1808(1):415-423. doi:10.1016/j.bbamem.2010.09.014.
 67. Wang T, Cady SD, Hong M. NMR Determination of Protein Partitioning into Membrane Domains with Different Curvatures and Application to the Influenza M2 Peptide. *Biophys J*. 2012;102(4):787-794. doi:10.1016/j.bpj.2012.01.010.
 68. Cady S, Wang T, Hong M. Membrane-Dependent Effects of a Cytoplasmic Helix on the Structure and Drug Binding of the Influenza Virus M2 Protein. *J Am Chem Soc*. 2011;133(30):11572-11579. doi:10.1021/ja202051n.
 69. Cady SD, Schmidt-Rohr K, Wang J, Soto CS, DeGrado WF, Hong M. Structure of the amantadine binding site of influenza M2 proton channels in lipid bilayers. *Nature*. 2010;463(7281):689-692. doi:10.1038/nature08722.
 70. Luo W, Cady SD, Hong M. Immobilization of the Influenza A M2 Transmembrane Peptide in Virus Envelope-Mimetic Lipid Membranes: A Solid-State NMR Investigation. *Biochemistry*. 2009;48(27):6361-6368. doi:10.1021/bi900716s.
 71. Carpenter T, Bond PJ, Khalid S, Sansom MSP. Self-Assembly of a Simple Membrane Protein: Coarse-Grained Molecular Dynamics Simulations of the Influenza M2 Channel. *Biophys J*. 2008;95(8):3790-3801. doi:10.1529/biophysj.108.131078.
 72. Wang T, Hong M. Investigation of the Curvature Induction and Membrane Localization of the Influenza Virus M2 Protein Using Static and Off-Magic-Angle Spinning Solid-State NMR of Oriented Bicelles. *Biochemistry*. 2015;54(13):2214-2226. doi:10.1021/acs.biochem.5b00127.
 73. Ho CS, Khadka NK, She F, Cai J, Pan J. Influenza M2 Transmembrane Domain Senses Membrane Heterogeneity and Enhances Membrane Curvature. *Langmuir*. 2016;32(26):6730-6738. doi:10.1021/acs.langmuir.6b00150.
 74. Chen Z, Rand RP. The influence of cholesterol on phospholipid membrane curvature and bending elasticity. *Biophys J*. 1997;73(1):267-276. doi:10.1016/S0006-3495(97)78067-6.
 75. Cullis PR, Van Dijck PWM, De Kruijff B, De Gier J. Effects of cholesterol on the properties of equimolar mixtures of synthetic phosphatidylethanolamine and phosphatidylcholine. A ³¹P NMR and differential scanning calorimetry study. *BBA - Biomembr*. 1978;513(1):21-30. doi:10.1016/0005-2736(78)90108-6.
 76. Cullis PR, De Kruijff B. Polymorphic phase behaviour of lipid mixtures as detected by ³¹P NMR. Evidence that cholesterol may destabilize bilayer structure in membrane systems containing phosphatidylethanolamine. *BBA - Biomembr*. 1978;507(2):207-218. doi:10.1016/0005-2736(78)90417-0.
 77. van Dijck PW, de Kruijff B, Verkley AJ, van Deenen LL, de Gier J. Comparative

- studies on the effects of pH and Ca²⁺ on bilayers of various negatively charged phospholipids and their mixtures with phosphatidylcholine. *Biochim Biophys Acta*. 1978;512(1):84-96. doi:10.1016/0005-2736(78)90219-5.
78. Helfrich W. Elastic Properties of Lipid Bilayers: Theory and Possible Experiments. *Zeitschrift für Naturforsch C*. 1973;28(11-12):693-703. doi:10.1515/znc-1973-11-1209.
 79. Gruner SM. Intrinsic curvature hypothesis for biomembrane lipid composition: a role for nonbilayer lipids. *Proc Natl Acad Sci U S A*. 1985;82(11):3665-3669. <http://www.ncbi.nlm.nih.gov/pubmed/3858841>. Accessed April 8, 2017.
 80. Botelho AV, Gibson NJ, Thurmond RL, Wang Y, Brown MF. Conformational energetics of rhodopsin modulated by nonlamellar-forming lipids. *Biochemistry*. 2002;41(20):6354-6368. doi:10.1021/bi011995g.
 81. Anderson DM, Gruner SM, Leibler S. Geometrical aspects of the frustration in the cubic phases of lyotropic liquid crystals. *Proc Natl Acad Sci U S A*. 1988;85(15):5364-5368. <http://www.ncbi.nlm.nih.gov/pubmed/3399497>. Accessed April 6, 2017.
 82. Marsh D. Lateral pressure profile, spontaneous curvature frustration, and the incorporation and conformation of proteins in membranes. *Biophys J*. 2007;93(11):3884-3899. doi:10.1529/biophysj.107.107938.
 83. Marsh D. Protein modulation of lipids, and vice-versa, in membranes. *Biochim Biophys Acta - Biomembr*. 2008;1778(7):1545-1575. doi:10.1016/j.bbamem.2008.01.015.
 84. Zheng H, Liu W, Anderson LY, Jiang Q-X. Lipid-dependent gating of a voltage-gated potassium channel. *Nat Commun*. 2011;2:250. doi:10.1038/ncomms1254.
 85. Keller SL, Bezrukov SM, Gruner SM, Tate MW, Vodyanoy I, Parsegian VA. Probability of alamethicin conductance states varies with nonlamellar tendency of bilayer phospholipids. *Biophys J*. 1993;65(1):23-27. doi:10.1016/S0006-3495(93)81040-3.
 86. Cantor RS. Lipid Composition and the Lateral Pressure Profile in Bilayers. *Biophys J*. 1999;76(5):2625-2639. doi:10.1016/S0006-3495(99)77415-1.
 87. Fantini J, Barrantes FJ. How cholesterol interacts with membrane proteins: an exploration of cholesterol-binding sites including CRAC, CARC, and tilted domains. *Front Physiol*. 2013;4:31. doi:10.3389/fphys.2013.00031.
 88. Ekanayake EV, Fu R, Cross TA, et al. Structural Influences: Cholesterol, Drug, and Proton Binding to Full-Length Influenza A M2 Protein. *Biophys J*. 2016;110(6):1391-1399. doi:10.1016/j.bpj.2015.11.3529.
 89. Attard GS, Templer RH, Smith WS, Hunt AN, Jackowski S. Modulation of CTP:phosphocholine cytidyltransferase by membrane curvature elastic stress. *Proc Natl Acad Sci U S A*. 2000;97(16):9032-9036. doi:10.1073/pnas.160260697.
 90. Drin G, Antonny B. Amphipathic helices and membrane curvature. *FEBS Lett*. 2010;584(9):1840-1847. doi:10.1016/j.febslet.2009.10.022.
 91. Antonny B. Mechanisms of Membrane Curvature Sensing. *Annu Rev Biochem*. 2011;80(1):101-123. doi:10.1146/annurev-biochem-052809-155121.
 92. Shen H, Pirruccello M, De Camilli P. SnapShot: Membrane Curvature Sensors and Generators. *Cell*. 2012;150(6):1300-1300.e2. doi:10.1016/j.cell.2012.08.017.
 93. Martyna A, Gómez-Llobregat J, Lindén M, Rossman JS. Curvature Sensing by a Viral Scission Protein. *Biochemistry*. 2016;55(25):3493-3496.

- doi:10.1021/acs.biochem.6b00539.
94. Martyna A, Bahsoun B, Badham MD, Srinivasan S, Howard MJ, Rossman JS. Membrane remodeling by the M2 amphipathic helix drives influenza virus membrane scission. *Sci Rep*. 2017;7:44695. doi:10.1038/srep44695.
 95. Campelo F, McMahon HT, Kozlov MM. The Hydrophobic Insertion Mechanism of Membrane Curvature Generation by Proteins. *Biophys J*. 2008;95(5):2325-2339. doi:10.1529/biophysj.108.133173.
 96. Campelo F, Malhotra V. Membrane Fission: The Biogenesis of Transport Carriers. *Annu Rev Biochem*. 2012;81(1):407-427. doi:10.1146/annurev-biochem-051710-094912.
 97. Snead WT, Hayden CC, Gadok AK, et al. Membrane fission by protein crowding. *Proc Natl Acad Sci U S A*. April 2017:201616199. doi:10.1073/pnas.1616199114.
 98. Busch DJ, Houser JR, Hayden CC, Sherman MB, Lafer EM, Stachowiak JC. Intrinsically disordered proteins drive membrane curvature. *Nat Commun*. 2015;6:7875. doi:10.1038/ncomms8875.
 99. Rossman JS, Lamb RA. Influenza Virus Assembly and Budding. *Virology*. 2011;411(2):229-236. doi:10.1016/j.virol.2010.12.003.